BUKTI SUBMIT MANUSKRIP

PENULIS MERUPAKAN PENULIS PERTAMA DAN SELALU BERKOMUNIKASI DENGAN KOREPONDING AUTHOR SELAMA PROSES PUBLIKASI, SEBAGAIMANA TERLAMPIR

Universitas Hasanuddin

Andi Dian Permana <andi.dian.permana@farmasi.unhas.ac.id>

Fwd: Track your recent Co-Authored submission to IJP

1 message

Andi Permana <apermana01@qub.ac.uk> Tue, Apr 4, 2023 at 3:52 PM
To: Andi Dian Permana <andi.dian.permana@farmasi.unhas.ac.id>

Get Outlook for iOS

From: eesserver@eesmail.elsevier.com <eesserver@eesmail.elsevier.com> on behalf of International Journal of Pharmaceutics <eesserver@eesmail.elsevier.com>
Sent: Saturday, December 14, 2019 6:06:32 AM
To: Andi Permana <apermana01@qub.ac.uk>
Subject: Track your recent Co-Authored submission to IJP

*** Automated email sent by the system ***

Dear Dr. Andi Dian Permana,

You have been listed as a Co-Author of the following submission:

Journal: International Journal of Pharmaceutics
Title: Bacterially sensitive nanoparticle-based dissolving microneedles of doxycycline for enhanced treatment of bacterial biofilm skin infection
Corresponding Author: Ryan Donnelly
Co-Authors: Andi Dian Permana; Maria Mir; Emilia Utomo;

To be kept informed of the status of your submission, register or log in (if you already have an Elsevier profile).

Register here: https://ees.elsevier.com/ijp/default.asp?acw=&pg=preRegistration.asp&user=coauthor&fname=Andi Dian&lname=Permana&email=apermana01@qub.ac.uk

Or log in: https://ees.elsevier.com/ijp/default.asp?acw=&pg=login.asp&email=apermana01@qub.ac.uk

If you did not co-author this submission, please do not follow the above link but instead contact the Corresponding Author of this submission at r.donnelly@qub.ac.uk.

Thank you,

International Journal of Pharmaceutics

BUKTI REVIEW DARI REVIEWERS

Universitas Hasanuddin

Andi Dian Permana <andi.dian.permana@farmasi.unhas.ac.id>

Fwd: Your Submission IJP-D-19-02770

1 message

Andi Permana <apermana01@qub.ac.uk> Tue, Apr 4, 2023 at 3:50 PM
To: Andi Dian Permana <andi.dian.permana@farmasi.unhas.ac.id>

Get Outlook for iOS

From: Ryan Donnelly <R.Donnelly@qub.ac.uk>
Sent: Monday, January 6, 2020 3:35:56 AM
To: Andi Permana <apermana01@qub.ac.uk>
Subject: FW: Your Submission IJP-D-19-02770

Great to see you on Skype yesterday Dian,

Please see below.

This is good news, I think.

Just in case you need to access the journal webpages in preparing the revision, my new password (after Elsevier had locked me outr of EJPB!) is:

Johanne@1977

Username is still my email address.

Happy to help in answering the reviewers' comments, so do let me know.

Well done again, Ronaldo!

Talk to you again soon.

Ryan

Professor Ryan F. Donnelly
Chair in Pharmaceutical Technology
School of Pharmacy
Queen's University Belfast
Medical Biology Centre
97 Lisburn Road
Belfast
BT9 7BL
UK
Tel: +44 (0) 2890 972 251
Fax: +44 (0) 2890 247 794
Email: r.donnelly@qub.ac.uk

From: eesserver@eesmail.elsevier.com <eesserver@eesmail.elsevier.com> on behalf of International Journal of Pharmaceutics <eesserver@eesmail.elsevier.com>
Sent: 05 January 2020 16:39
To: Ryan Donnelly
Subject: Your Submission IJP-D-19-02770

This message is from an external sender. Please take care when responding, clicking links or opening attachments.

Ms. Ref. No.: IJP-D-19-02770
Title: Bacterially sensitive nanoparticle-based dissolving microneedles of doxycycline for enhanced treatment of bacterial biofilm skin infection
International Journal of Pharmaceutics or its open access mirror

Dear Dr. Donnelly,

Comments on your paper have now been received and are attached to this message. Please consider all the points made and upon returning your paper detail your responses and the actions taken.

Please submit the revised manuscript by Mar 05, 2020. Upon receipt of your revised paper, we will inform you of the outcome as soon as possible. Papers not received within that that time period will be considered to be withdrawn, you are welcome to resubmit your paper as a new submission at a later date.

NOTE: While submitting the revised manuscript, please double check the author names provided in the submission so that authorship related changes are made in the revision stage. If your manuscript is accepted, any authorship change will involve approval from co-authors and respective editor handling the submission and this may cause a significant delay in publishing your manuscript.

PLEASE NOTE: International Journal of Pharmaceutics or its open access mirror would like to invite you to enrich your article by including a list of up to 10 names of chemical compounds studied in the article.

Include interactive data visualizations in your publication and let your readers interact and engage more closely with your research. Follow the instructions here: https://www.elsevier.com/authors/author-services/data-visualization to find out about available data visualization options and how to include them with your article.

Thank you for submitting your work to the journal.

MethodsX file (optional)
We invite you to submit a method article alongside your research article. This is an opportunity to get full credit for the time and money you have spent on developing research methods, and to increase the visibility and impact of your work. If your research article is accepted, your method article will be automatically transferred over to the open access journal, MethodsX, where it will be editorially reviewed and published as a separate method article upon acceptance. Both articles will be linked on ScienceDirect. Please use the MethodsX template available here when preparing your article: https://www.elsevier.com/MethodsX-template. Open access fees apply.

Yours sincerely,

Juergen Siepmann, PhD
Editor-in-Chief
International Journal of Pharmaceutics or its open access mirror

p.s. To submit a revision, please go to http://ees.elsevier.com/ijp/ and login as an Author.

Your username is: r.donnelly@qub.ac.uk
If you need to retrieve password details, please go to: http://ees.elsevier.com/ijp/automail_query.asp
On your Main Menu page is a folder entitled "Submissions Needing Revision". You will find your submission record there.

Reviewers' comments:

Reviewer #1: Nice paper, expanding further the range of molecules that may be delivered with microneedle technology.Also, good to see the problem of wound healing being addressed.

A comprehensive set of experiments supports the major conclusions.

I would encourage the authors to comment on why chitosan has not really made an impact on dosaage forms despite many papers and publications highlighting the utility of this biomaterial.

Could the authors explain in more detail how the tissue was applied aseptically to the TSA plates?

Please note that there are some minor typographical errors in the text.

The resolution of Figure 1 should be improved if possible.

Reviewer #2: This paper presents the preparation, characterization and ex-vivo evaluation of doxycycline loaded nanoparticle entrapped in microneedle patch against S. aureus and P. aeruginosa biofilms.

* Introduction section is weak in narration of the importance of this work. Especially, authors should make a strong case for utilization of microneedle devices for application on wounds, where there is no physical barrier. Biofilm cannot be considered as a barrier that microneedles should be inserted into.
* Furthermore, the argument that PLGA and PCL nanoparticles would get hydrolyzed by bacterial enzymes thereby allowing targeting is not convincing as the delivery method is localized, where the nanoparticles or nanoparticle within MN were directly applied on the biofilm.
* Page 13, the needle tip dimension 600µm may not be correct.
* A representative photograph of MN inserted in ex-vivo biofilm model needs to be provided. How long will it take for the MN to get dissolved in biofilm?
* Authors should validate the biofilm characteristics obtained in ex-vivo model to that found in in-vivo models.
* The information provided by FTIR spectroscopy is limited when a drug compound was encapsulated in polymeric nanoparticles. Instead, powder XRD and DSC would provide if compound is in crystalline state or amorphous which can be related to release kinetic models. Furthermore, molecular modeling would provide the nature of interactions among excipients and DOX that would influence release kinetics.
* The number of Figures could be reduced. Few cases there was same data presented in different format (example Figure 2, 3).
* None of the Figures and Tables provide statistical analysis information.
* Table 3, zero-values in few boxes may not be appropriate.
* Table S5-S9, include units of measurements.
* The data provided would be sufficient to claim "proof-of-concept."
* The claims of DOX release in response to lipase enzyme seems to be speculative.

Reviewer #3:

My key concern is the following:

The authors fitted the experimental drug release data to different mathematical models to analyse the drug release mechanisms. Unfortunately, the applied models are empirical or semi-empirical. So, mechanistic conclusions are not justified, e.g. "Therefore, the mechanism of release of DOX from NPs was considered to be non-Fickian (anomalous diffusion)…'".
This mathematical analysis should be omitted, since it does not offer new insight: it is purely descriptive. The paper is much more straightforward without.

Comment from the editor:

The resolution of Figure 1 is fine in the Word file you uploaded. The transformation into the pdf file decreased the resolution. Please double check this aspect at the galley proof stage.

Data in Brief (optional):

We invite you to convert your supplementary data (or a part of it) into an additional journal publication in Data in Brief, a multi-disciplinary open access journal. Data in Brief articles are a fantastic way to describe supplementary data and associated metadata, or full raw datasets deposited in an external repository, which are otherwise unnoticed. A Data in Brief article (which will be reviewed, formatted, indexed, and given a DOI) will make your data easier to find, reproduce, and cite.

You can submit to Data in Brief via the International Journal of Pharmaceutics or its open access mirror submission system when you upload your revised International Journal of Pharmaceutics or its open access mirror manuscript. To do so, complete the template and follow the co-submission instructions found here: www.elsevier.com/dib-template. If your International Journal of Pharmaceutics or its open access mirror manuscript is accepted, your Data in Brief submission will automatically be transferred to Data in Brief for editorial review and publication.

Please note: an open access Article Publication Charge (APC) is payable by the author or research funder to cover the costs associated with publication in Data in Brief and ensure your data article is immediately and permanently free to access by all. For the current APC see: www.elsevier.com/journals/data-in-brief/2352-3409/open-access-journal

Please contact the Data in Brief editorial office at dib-me@elsevier.com or visit the Data in Brief homepage (www.journals.elsevier.com/data-in-brief/) if you have questions or need further information.

For further assistance, please visit our customer support site at http://help.elsevier.com/app/answers/list/p/7923. Here you can search for solutions on a range of topics, find answers to frequently asked questions and learn more about EES via interactive tutorials. You will also find our 24/7 support contact details should you need any further assistance from one of our customer support representatives.

BUKTI SUBMIT HASIL REVIEW

Ms. Ref. No.: IJP-D-19-02770

Title: Bacterially sensitive nanoparticle-based dissolving microneedles of doxycycline for enhanced treatment of bacterial biofilm skin infection

Response to Reviewers

We are very thankful to the expert reviewers for taking the time to kindly review our manuscript and provide helpful comments for improvement and clarification. We have made some changes to the manuscript as a result of these comments. We believe that the manuscript is now substantially improved. We have addressed each of the reviewers' comments in detail below.

Reviewers' comments:

Reviewer #1: Nice paper, expanding further the range of molecules that may be delivered with microneedle technology.Also, good to see the problem of wound healing being addressed.

A comprehensive set of experiments supports the major conclusions.

Response: We thank the reviewer for reviewing the manuscript in detail and providing valuable suggestions for the improvement of our manuscript.

I would encourage the authors to comment on why chitosan has not really made an impact on dosaage forms despite many papers and publications highlighting the utility of this biomaterial.

Response:

We thank the reviewer for pointing out this part. Indeed, chitosan has exhibited a great antimicrobial activity. Our results in Table 3, Figure 2 and Figure 3 showed that the MIC and MBC values, antibiofilm activity in 96-well microtiter plate and colony biofilm models of chitosan NPs were higher compared to NPs without chitosan. However, our dermatokinetic studies (Section 3.9) showed that the skin retention profiles of DOX following the application of MNs containing NPs of combination of chitosan and either PLGA or PCL were significantly higher compared to MNs containing chitosan NPs. Therefore, the ability of MN-chitosan NPs in retaining DOX in the skin were lower than others MNs. Our study is supported by Özcan et al, (2013) comparing the skin retention of betamethasone valerate from PLGA and chitosan NPs. It was found that the concentration of this drug in dermis following the application of PLGA NPs was around 4-times higher in comparison with chitosan NPs (Özcan et al., 2013). We have added this explanation in our manuscript.

Özcan, I., Azizoğlu, E., Şenyiğit, T., Özyazici, M., Özer, Ö., 2013. Comparison of PLGA and lecithin/chitosan nanoparticles for dermal targeting of betamethasone valerate. J. Drug Target. 21, 542–550.

Could the authors explain in more detail how the tissue was applied aseptically to the TSA plates?

Response:

We thank the reviewer for the question. In this step, to avoid contamination, we performed the experiment in Class II Microbiological safety cabinet Technically, we moved the skin pieces

from one plate to another plate by a metal tweezer. We have mention this in our manuscript to improve the clarity.

Please note that there are some minor typographical errors in the text.

Response:

We thank the reviewer for pointing out this part. We have re-read the manuscript and made some changed appropriately.

The resolution of Figure 1 should be improved if possible.

Response:

As per the comment from the Editor, the resolution of Figure 1 is fine. The low resolution was caused by the transformation into pdf file.

Reviewer #2: This paper presents the preparation, characterization and ex-vivo evaluation of doxycycline loaded nanoparticle entrapped in microneedle patch against S. aureus and P. aeruginosa biofilms.

* Introduction section is weak in narration of the importance of this work. Especially, authors should make a strong case for utilization of microneedle devices for application on wounds, where there is no physical barrier. Biofilm cannot be considered as a barrier that microneedles should be inserted into.

Response:

We thank the reviewer for the comment. Indeed, we agreed that in wounds, there is no physical barrier. However, the presence of bacterial biofilms is another challenge in the treatment. It has been previously reported that biofilms are a bacteria an assemblage, connecting to the wound surface and cannot be eliminated by simple rinsing.

Current biofilm removal process utilizes bleach or other erosive compounds to sterilise the wound (Marion-Ferey et al., 2003), resulting in low patient compliance and high health care expenses (Lynch and Robertson, 2008). Removal debridement by surgery of infected wounds can completely eliminate biofilm of the wound area. Nevertheless, it has been reported that biofilms are observed again after 2 days of the first removal (Wolcott et al., 2010), and the long-term antibiotic treatment further increases the appearance of antibiotic-resistant bacteria (Levy and Bonnie, 2004).

Despite the fact that the nanocarriers have been broadly investigated for their efficacy in antimicrobial drug delivery, only a few investigations exist focusing on the delivery of nanoparticles to the biofilm. Additionally, as per our explanation in our manuscript, the presence of necrotic tissue overlying the wound bed is another challenge in treatment (Caffarel-Salvador et al., 2015). These terms explain the nature of the target site presenting a need of specialized delivery system, which is capable of overcoming these problems. Conventional topical dosage forms, i.e. creams, dressings and gels, have been reported to exhibit poor penetration of drug to this barrier, resulting in low drug concentration in the infected site. Hence, this description provides the benchmark for using this device.

Caffarel-Salvador, E., Kearney, M.C., Mairs, R., Gallo, L., Stewart, S.A., Brady, A.J., Donnelly, R.F., 2015. Methylene blue-loaded dissolving microneedles: Potential use

in photodynamic antimicrobial chemotherapy of infected wounds. Pharmaceutics 7, 397–412.

Levy, S.B., Bonnie, M., 2004. Antibacterial resistance worldwide: Causes, challenges and responses. Nat. Med. 10, S122− S129.

Lynch, A.S., Robertson, G.T., 2008. Bacterial and fungal biofilm infections. Annu. Rev. Med. 59, 415−428.

Marion-Ferey, K., Pasmore, M., Stoodley, P., Wilson, S., Husson, G.P., Costerton, J.W., 2003. Biofilm removal from silicone tubing: An assessment of the efficacy of dialysis machine decontamination procedures using an in vitro model. J. Hosp. Infect. 53, 64–71.

Wolcott, R.D., Rumbaugh, K.P., James, G., Schultz, G., Phillips, P., Yang, Q., Waiters, C., Stewart, P.S., Dowd, S.E., 2010. Biofilm maturity studies indicate sharp debridement opens a timedependent therapeutic window. J. Wound Care 19, 320−328.

* Furthermore, the argument that PLGA and PCL nanoparticles would get hydrolyzed by bacterial enzymes thereby allowing targeting is not convincing as the delivery method is localized, where the nanoparticles or nanoparticle within MN were directly applied on the biofilm.

Response:

We thank the reviewer for the comment. However, following our literature review which has been also explained in our manuscript, the selection of PLGA and PCL was based on the utilization of these polymers to be selectively hydrolyzed by bacteria, especially by *Staphylococcus aureus* and *Pseudomonas aeruginosa*. Therefore, we argued that the efficacy

of our approach was because of the hydrolysis of PLGA and PCL chain by bacteria, releasing DOX to the specific infected area. We have explained this in our manuscript:

> With respect to the selection of biodegradable polymers, it has been reported that lipolytic esterases produced by SA and PA were able to initiate the bicatalytic hydrolysis of poly(lactic-co-glycolic acid) (PLGA) in ultrafine fiber formulations (Said et al., 2012, 2011) and poly (Ɛ-caprolactone) (PCL) in nanogel formulations (Xiong et al., 2012). Therefore, these polymers can be considered as suitable polymers to selectively deliver antimicrobial agents to the infected site only.

With respect to the localized delivery method, our main purpose was to deliver nanoparticles directly to the biofilm. Due to the reason that we explained previously, it has been reported that biofilms are observed again after 2 days of the first removal. Therefore, the administration of drug nanoparticle directly to the biofilm, where the bacteria produce enzyme to hydrolize the polymers, would be beneficial to increase the effectiveness of skin infection therapy.

Additionally, our study showed that the release profile of DOX was significantly enhaced by the presence of bacteria. Importantly, following the administration of MN containing DOX-NPs in *ex vivo* skin infection model, the concentration of DOX released from was significantly higher in comparison with the concentration of DOX in normal skin. Thus, it implies that the release of DOX was affected by bacterial enzyme in infected skin after local administration of MNs.

Said, S.S., Aloufy, A.K., El-Halfawy, O.M., Boraei, N.A., El-Khordagui, L.K., 2011. Antimicrobial PLGA ultrafine fibers: Interaction with wound bacteria. Eur. J. Pharm. Biopharm. 79, 108–118.

Said, S.S., El-Halfawy, O.M., El-Gowelli, H.M., Aloufy, A.K., Boraei, N.A., El-Khordagui, L.K., 2012. Bioburden-responsive antimicrobial PLGA ultrafine fibers for wound healing. Eur. J. Pharm. Biopharm. 80, 85–94.

Xiong, M.H., Bao, Y., Yang, X.Z., Wang, Y.C., Sun, B., Wang, J., 2012. Lipase-sensitive polymeric triple-layered nanogel for "on-demand" drug delivery. J. Am. Chem. Soc. 134, 4355–4362.

* Page 13, the needle tip dimension 600µm may not be correct.

Response:

We thank the reviewer for the comment. The needle density of our MN moulds are 16 x 16, pyramidal needles; 850 µm height, consisting of 600 µm pyramidal tip, 250 µm base column. Therefore, 600 µm is correct dimension.

* A representative photograph of MN inserted in ex-vivo biofilm model needs to be provided. How long will it take for the MN to get dissolved in biofilm?

Response:

We thank the reviewer for the suggestion. We have now included this into our manuscript, showing that the MNs were completely dissolved in biofilm after 20 minutes.

* Authors should validate the biofilm characteristics obtained in ex-vivo model to that found in in-vivo models.

Response:

We thank the reviewer for the suggestion. In our manuscript, we have shown the SEM images of biofilm formed in our study. The images were similar to SEM images of bacterial biofilm in several studies (Iliescu Nelea et al., 2019; Li et al., 2020; Zhang et al., 2020). In addition, we have also performed the observation of biofilm formed in our *ex vivo* model using optical coherence tomography. This method has been applied to evaluate the formation of skin bacterial biofilm *in vivo* (Mohan et al., 2019). We have included this results in our manuscript.

Iliescu Nelea, M., Paek, L., Dao, L., Rouchet, N., Efanov, J.I., Édouard, C., Danino, M.A., 2019. In-situ characterization of the bacterial biofilm associated with Xeroform™ and Kaltostat™ dressings and evaluation of their effectiveness on thin skin engraftment donor sites in burn patients. Burns 45, 1122–1130.

Li, Y., Feng, S., Liu, H., Tian, X., Xia, Y., Li, M., Xu, K., Yu, H., Liu, Q., Chen, C., 2020. Bacterial distribution in SRB biofilm affects MIC pitting of carbon steel studied using FIB-SEM. Corros. Sci.

Mohan, M., Nigam, V.K., Poddar, R., 2019. Towards characterization of bacterial colonies and biofilms: An approach based on swept source optical coherence tomography. Optik (Stuttg). 185, 592–598.

Zhang, Z.Y., Sun, Y., Zheng, Y.D., He, W., Yang, Y.Y., Xie, Y.J., Feng, Z.X., Qiao, K., 2020. A biocompatible bacterial cellulose/tannic acid composite with antibacterial and anti-biofilm activities for biomedical applications. Mater. Sci. Eng. C 106, 110249.

* The information provided by FTIR spectroscopy is limited when a drug compound was encapsulated in polymeric nanoparticles. Instead, powder XRD and DSC would provide if compound is in crystalline state or amorphous which can be related to release kinetic models. Furthermore, molecular modeling would provide the nature of interactions among excipients and DOX that would influence release kinetics.

Response:

We thank the reviewer for the suggestion. Following the reviewer suggestion, we have performed XRD and DSC studies and included the results in our manuscript. The detail of these results is explained in the manuscript.

* The number of Figures could be reduced. Few cases there was same data presented in different format (example Figure 2, 3).

Response:

We thank the reviewer for the suggestion. We have reduced the number of Figures by combining the OCT images of insertion profile of MNs and mechanical properties of MNs. However, with respect to Figure 2 and 3, they are completely different studies. Figure 2 shows Time kill assay and antibiofilm activity in 96-well microtiter plate of DOX and DOX-loaded NPs. While Figure 3 presents antibiofilm activity of DOX, DOX-loaded NPs and blank NPs in colony biofilm model, as well as *in vitro* drug release of DOX from NPs in the absence and presence of bacterial culture. Accordingly, it was not possible to combine these results.

* None of the Figures and Tables provide statistical analysis information.

Response:

We thank the reviewer for the comment. We have now included the statistical results in all sections discussing the Figures and Tables.

* Table 3, zero-values in few boxes may not be appropriate.

Response:

Thanks for the suggestion. Needful is done.

* Table S5-S9, include units of measurements.

Response:

Thanks for the suggestion. Needful is done.

* The data provided would be sufficient to claim "proof-of-concept."

Response:

We thank the reviewer for the suggestion. We have included the term of “proof-of-concept” in our manuscript title.

* The claims of DOX release in response to lipase enzyme seems to be speculative.

Response:

We thank the reviewer for the comment. As per our response in previous comment, the selection of PLGA and PCL was based on the utilization of these polymers to be selectively hydrolyzed by bacteria, especially by *Staphylococcus aureus* and *Pseudomonas aeruginosa*. Therefore, we argued that the efficacy of our approach was because of the hydrolysis of PLGA and PCL chain by bacteria, releasing DOX to the specific infected area. We have explained this in our manuscript:

> With respect to the selection of biodegradable polymers, it has been reported that lipolytic esterases produced by SA and PA were able to initiate the bicatalytic hydrolysis of poly(lactic-co-glycolic acid) (PLGA) in ultrafine fiber formulations (Said et al., 2012, 2011) and poly (Ɛ-caprolactone) (PCL) in nanogel formulations (Xiong et al., 2012). Therefore, these polymers can be considered as suitable polymers to selectively deliver antimicrobial agents to the infected site only.

Said, S.S., Aloufy, A.K., El-Halfawy, O.M., Boraei, N.A., El-Khordagui, L.K., 2011. Antimicrobial PLGA ultrafine fibers: Interaction with wound bacteria. Eur. J. Pharm. Biopharm. 79, 108–118.

Said, S.S., El-Halfawy, O.M., El-Gowelli, H.M., Aloufy, A.K., Boraei, N.A., El-Khordagui, L.K., 2012. Bioburden-responsive antimicrobial PLGA ultrafine fibers

for wound healing. Eur. J. Pharm. Biopharm. 80, 85–94.

Xiong, M.H., Bao, Y., Yang, X.Z., Wang, Y.C., Sun, B., Wang, J., 2012. Lipase-sensitive polymeric triple-layered nanogel for "on-demand" drug delivery. J. Am. Chem. Soc. 134, 4355–4362.

Reviewer #3:

My key concern is the following:

The authors fitted the experimental drug release data to different mathematical models to analyse the drug release mechanisms. Unfortunately, the applied models are empirical or semi-empirical. So, mechanistic conclusions are not justified, e.g. "Therefore, the mechanism of release of DOX from NPs was considered to be non-Fickian (anomalous diffusion)…'". This mathematical analysis should be omitted, since it does not offer new insight: it is purely descriptive. The paper is much more straightforward without.

Response:

We thank the reviewer for the suggestion. We have removed the kinetic mathematic models as per request from the reviewer.

Bacterially sensitive nanoparticle-based dissolving microneedles of doxycycline for enhanced treatment of bacterial biofilm skin infection: A proof of concept study

Andi Dian Permana[1,2], Maria Mir[1,3], Emilia Utomo[1], Ryan F. Donnelly[1*]

1. School of Pharmacy, Queen's University Belfast, Medical Biology Centre, 97 Lisburn Road, Belfast. BT9 7BL, UK

2. Department of Pharmaceutics, Faculty of Pharmacy, Hasanuddin University, Makassar, Indonesia

3. Department of Pharmacy, Faculty of Biological Sciences, Quaid-i-Azam University, Islamabad 45320, Pakistan

***Corresponding author:**
Professor Ryan F. Donnelly
Chair in Pharmaceutical Technology
School of Pharmacy
Queens University Belfast
Medical Biology Centre
97 Lisburn Road
Belfast
BT9 7BL, Northern Ireland
United Kingdom
Tel: +44 (0) 28 90 972 251
Fax: +44 (0) 28 90 247 794
Email: r.donnelly@qub.ac.uk

ABSTRACT

The presence of bacterial biofilms in wounds is a main issue in the healing process. Conventional therapy of bacterial biofilms is hampered by the poor penetration of antibacterial agents through the physical barrier on the infected skin and the non-specific target of antibacterial agents. Here, we present a combination approach of bacterial sensitive nanoparticles (NPs) and dissolving microneedles (MNs) of doxycycline (DOX) for improved biofilm penetration and specifically delivering DOX to the infection site. The NPs were prepared from poly(lactic-co-glycolic acid) and poly (Ɛ-caprolactone) decorated with chitosan. The release of DOX was improved with the presence of bacterial producing biofilm up to 7-fold. The incorporation of these NPs into dissolving MNs was able to significantly enhance the dermatokinetic profiles of DOX, indicated by higher retention time compared to needle-free patches. Importantly, the antibiofilm activity in *ex vivo* biofilm model showed that after 48 h, the bacterial bioburdens decreased up to 99.99% following the application of this approach. The results presented here assist as proof of principle for the improvement of dermatokinetic profiles and antibiofilm activities of DOX, following its formulation into bacterial sensitive NPs and delivery *via* MN. Future studies must explore *in vivo* efficacy in a suitable animal model.

KEYWORDS

Doxycycline; nanoparticles; biofilm; microneedles; *Staphylococcus aureus*; *Pseudomonas aeruginosa*.

1. Introduction

Burn and chronic wounds are difficult to heal and need extended management thanks to several clinical complications (Alhusein et al., 2016; Hammond et al., 2011; Moore et al., 2006). Additionally, they significantly affect life quality of patients and are one of the main health concern for care systems globally. Importantly, it has been reported that approximately $50 billion are consumed per annum on care management of chronic wounds (El-Mohri et al., 2017). In addition to surgical debridement (including necrotic and infected tissue removal), the systemic and/or topical administration of antimicrobial agents for an extended period of time as the most recent therapeutic strategy for burn and chronic wounds could result in undesired systemic side effects (Haidar et al., 2020; Mihai et al., 2018). Furthermore, over approximately 80% of chronic wounds are assumed to be related with biofilm formation of bacteria (Duckworth et al., 2018). Despite the fact that several bacterial pathogens are involved, *Staphylococcus aureus* (SA) and *Pseudomonas aeruginosa* (PA) are the most commonly-isolated pathogens (Clinmicrorevs et al., 2001; Doern et al., 1999).

Bacterial biofilms are defined as a multifarious bacterial communities attached as aggregates and surrounded within polysaccharides, adhesive pili, extracellular DNA, lipids and protein, referred to as a self-synthesized matrix of hydrated extracellular polymeric substances (EPS) (Flemming and Wingender, 2010; Olsen, 2015). In these cases, due to the fact that planktonic bacteria encapsulated in a biofilm matrix can display up to 1000-times more antibiotic resistance, conventional antibiotic treatments are often unsuccessful (Olsen, 2015). Unsurprisingly, since the currently used antibiotics have been primarily used to target planktonic bacteria, they are, therefore, unsuccessful in eliminating biofilm bacteria (Parsons and Summers, 2017). Importantly, biofilms have been recognized as a key impediment to the process of wound healing (Duckworth

et al., 2018). Current biofilm removal process utilizes bleach or other erosive compounds to sterilise the wound (Marion-Ferey et al., 2003), resulting in low patient compliance and high health care expenses(Lynch and Robertson, 2008). Removal debridement by surgery of infected wounds can completely eliminate biofilm of the wound area. Nevertheless, it has been reported that biofilms are observed again after 2 days of the first removal (Wolcott et al., 2010), and the long-term antibiotic treatment further increases the appearance of antibiotic-resistant bacteria (Levy and Bonnie, 2004). Accordingly, the development of a novel drug delivery system as therapeutic chronic wound management which can disrupt and kill the bacterial biofilm is urgently warranted.

Several antimicrobial agents have been widely used in burn and chronic wounds. Doxycycline (DOX) is one of the agents which can effectively kill SA and PA (Adhirajan et al., 2009; Sader et al., 2002). The utilization of biodegradable nanoparticles (NPs) has been considered as a promising antimicrobial approach for efficient therapeutic management of infection (Guo et al., 2016). In order to improve the effectiveness of therapeutic agent, the NPs formulation have been modified by enhancing the targeting efficiency or responding to adjacent inducements, i.e. enzyme, pH or temperature (Allen and Cullis, 2004). With respect to the selection of biodegradable polymers, it has been reported that lipolytic esterases produced by SA and PA were able to initiate the bicatalytic hydrolysis of poly(lactic-co-glycolic acid) (PLGA) in ultrafine fiber formulations (Said et al., 2012, 2011) and poly (Ɛ-caprolactone) (PCL) in nanogel formulations (Xiong et al., 2012). Therefore, these polymers can be considered as suitable polymers to selectively deliver antimicrobial agents to the infected site only. As a result, this delivery could potentially reduce the exposure to undesired sites, leading to a safe treatment strategy. Lately, the decoration of NPs charge with specific ligands have been conducted to modify the delivery of NPs. Amongst several types of ligands, chitosan is one of the generally used in NP formulations (Badran et al., 2018). In

terms of bacterial biofilm targeting, chitosan has been reported to be biocompatible and biodegradable, and to possess an antimicrobial activity (Rabea et al., 2003). Chitosan NPs have been successfully utilized against 24-h-old *P. aeruginosa* biofilms of six strains isolated from clinical studies (Machul et al., 2015). Chitosan NPs possess a positive surface charge, whereas the surfaces of biofilm EPS and bacterial cell walls are negative. Accordingly, chitosan is anticipated to exhibit a high attraction to infected areas (Han et al., 2017). Leading on from these, the incorporation of chitosan onto either a PLGA or a PCL surface could potentially increase the effectiveness of biofilm targeting.

To penetrate the dense physical obstacle that biofilms present, the choice of a suitable dosage form is crucial. The systemic administration of antimicrobial agents is not able to deliver the drugs successfully to the desired infection site (Noel et al., 2010). Interestingly, in burn and chronic wounds, in addition to biofilm, the presence of necrotic tissue overlying the wound bed is another challenge in treatment (Caffarel-Salvador et al., 2015). Conventional topical dosage forms, i.e. creams, dressings and gels, have been reported to exhibit poor penetration of drug to this barrier, resulting in low drug concentration in the infected site (Bharambe et al., 2013; Lipsky and Hoey, 2009). Despite the fact that the nanocarriers have been broadly investigated for their efficacy in antimicrobial drug delivery, only a few investigations exist focusing on the delivery of nanoparticles to the biofilm. With this in mind, a new drug device which can increase the penetrability of antimicrobials across the necrotic tissue is required. This would avoid the necessity of necrotic tissue removal before the application of the conventional dosage forms, mentioned previously, in clinics. Dissolving microneedles (MNs) are a drug device which can by-pass the major skin barrier (Permana et al., 2019a). Essentially, MNs can provide a painless, localized, rapid delivery and patient-compliant administration approach. Unlike hypodermic needle

injections, dissolving MNs are self-dissolvable and are prepared from biocompatible and biodegradable polymers. Thus, their utilization does not produce any biohazardous sharps waste (Permana et al., 2019c). Considering the advantages of this technology, the incorporation of NPs into dissolving MNs could potentially improve the amount of NPS penetrating the necrotic tissue of infected skin, and, as such, could potentially increase the effectiveness of burns and chronic wound management.

In this study, we present, for the first time, the development of NPs loaded with DOX incorporated into dissolving MNs as an innovative approach for potential improved treatment of chronic wounds with bacterial biofilms. PLGA and PCL were utilized as the polymer matrixes of the NPs, coated with chitosan to produce positively charged NPs. The NPs were characterized for their size, polydispersity index, zeta potential, shape, antibacterial activities and antibiofilm activities. Specifically, the release behavior of DOX in NPs was carried out with and without the presence of bacteria commonly associated with chronic wounds, namely SA and PA. Following this, the NPs were further loaded into dissolving MNs and the MNs were assessed for mechanical and insertion properties. Furthermore, to evaluate the effectiveness this approach, *ex vivo* dermatokinetic studies were carried out in normal porcine skin and *ex vivo* neonatal porcine skin biofilm model. Finally, the ability to penetrate and kill the bacterial biofilms were performed in *ex vivo* skin biofilm model. This is the first study investigating the effectiveness of the combination approach of NPs and MNs in *ex vivo* porcine skin biofilm model. The results of these proof of concept studies point towards the potential utilization of this combination delivery system to overcome the challenge in the treatment of bacterial biofilm infections in the skin.

2. Materials and methods

2.1. Materials

Doxycycline hyclate (DOX) (purity, ≥98%) of analytical grade was purchased from Alfa Aesar (Lancashire, UK). Acetic acid, chitosan (low-molecular-weight: 50–190 kDa), dichloromethane (DCM), poly(vinyl alcohol) (PVA) (31–50 kDa), PVA (9–10 kDa), poly (Ɛ-caprolactone) (PCL) (45 kDa) and sodium tripolyphosphate (TPP) were purchased from Sigma-Aldrich (Dorset, UK). Poly(lactic-co-glycolic acid) 40-75 kDa) was purchased from Lakeshore Biomaterials (Birmingham, AL). Poly(vinylpyrrolidone) PVP (58 kDa) was provided by Ashland (Kidderminster, UK). Ultrapure water was obtained from a water purification system (Elga PURELAB DV 25, Veolia Water Systems, Dublin, Ireland). All other reagents were of analytical grade and purchased from standard commercial suppliers.

2.2. Formulation of DOX-loaded NPs

A double emulsion (water-in-oil-in water) (W/O/W) solvent evaporation method was applied to prepare DOX loaded PLGA (NP-1) and PCL NPs (NP-2) (Badran et al., 2018). Table 1 shows the composition of the NPs. In brief, DOX solution in water (1 mL) was emulsified in PLGA or PCL solution in dichloromethane (DCM) (2 mL) in a probe sonicator (at an amplitude of 80% with 10 s pulse on and 5 s pulse off) for 1 min, producing a water-in-oil (W/O) emulsion. Afterwards, this emulsion was emulsified in 5 mL PVA (9-10 kDa) solution in water (2% w/v) in a probe sonicator (at an amplitude of 80% with 10 s pulse on and 5 s pulse off) for 5 min, forming a W/O/W emulsion. To remove the DCM, this double emulsion was stirred for 6 h at room temperature. Finally, the formed NPs were collected after three washing cycles with distilled water by

centrifugation at 14,000 rpm (Sigma® 1–14 micro-centrifuge, SciQuip Ltd., Shropshire, UK) for 30 min to remove the free DOX and the PVA solution.

To prepare PLGA (NP-3) and PCL (NP-4) NPs-coated with chitosan, NPs pellets collected after washing were dispersed in 5 mL distilled water. These dispersions were further mixed with the same volume of chitosan solutions (in 0.5% v/v acetic acid). The mixtures were then stirred for 2 h to allow the formation of NPs-coated chitosan. The formed NPs-coated chitosan was collected using the same procedure as uncoated NPs.

The chitosan NPs (NP-5) were prepared by an ionotropic gelation technique (Mili et al., 2018), with slight modifications. DOX and tripolyphosphate (TPP) were dissolved in distilled water. This solution was gently added to chitosan solution in 0.5% v/v acetic acid (in water) while stirred at 1,000 rpm at room temperature post addition for 1 h. The formed NPs were collected using the same protocols as the PLGA and PCL NPs.

Table 1. Composition of formulations NPs laded with DOX.

Composition	NP-1	NP-2	NP-3	NP-4	NP-5
PLGA (mg/2 mL)	50	-	50	-	-
PCL (mg/2 mL)	-	50	-	50	-
Chitosan (mg/5 mL)	-	-	50	50	50
TPP (mg/2.5 mL)	-	-	-	-	25
DOX (mg/mL)	25	25	25	25	25

2.3. Characterization of DOX-loaded NPs

The particle sizes, polydispersity indices (PDI) and zeta potentials were determined using a NanoBrook Omni particle sizer and zeta potential analyser (Brookhaven, New York, USA).

The encapsulations efficiency (EE) of DOX in NPs formulations were quantified by an indirect method (Badran et al., 2018). The amount of free DOX in the supernatant, following three washing

cycles, was quantified using the HPLC method described in the analytical section. Finally, the EE of DOX was calculated using Equation (1).

$$\text{EE (\%)} = \frac{DOX_{total} - DOX_{free}}{DOX_{total}} \; x \; 100\% \qquad \text{Equation (1)}$$

To determine the drug loading (DL%) of DOX in NPs formulations, NPs dispersions were freeze dried (Virtis Advantage Bench-top Freeze-drier system, SP Scientific, Warminster, PA, USA) for 24 h, forming dry NPs. For PLGA NPs, PCL NPs as well as PLGA and PCL NPs-coated with chitosan, 10 mg of freeze-dried NPs was firstly dispersed in 5 mL of distilled water. Acetone (2 mL) was added to the dispersion to disrupt the NPs and the mixture was sonicated in a bath sonicator for 1 h. For chitosan NPs, 10 mg of freeze-dried NPs was dissolved in 10 mL of acetic acid solution (0.5% v/v) and was sonicated in a bath sonicator for 1 h. The suspension was then centrifuged at 14,000 rpm for 15 min and the amount of DOX in supernatant was quantified by HPLC. The DL was calculated using Equation (2).

$$\text{DL (\%)} = \frac{Amount\ of\ encapsulated\ DOX}{Total\ weight} \; x \; 100\% \qquad \text{Equation (2)}$$

The morphologies of the DOX-loaded NPs were investigated using a scanning electron microscope (SEM) TM3030 (Hitachi, Krefeld, Germany). The interactions between each component in the formulations were studied using a Fourier transform infrared (FTIR) spectrometer (Accutrac FT/IR-4100™ Series, Jasco, Essex, UK). Differential scanning calorimetry (DSC) analysis of DOX, polymers, physical mixtures and DOX-loaded NPs were performed using a differential scanning calorimeter (DSC 2920, TA Instruments, Surry, UK). X-ray powder diffraction of DOX, polymers, physical mixtures and DOX-loaded NPs was carried out using a X-ray diffractometer (Rigaku Corporation, Kent, England).

2.4. In vitro antibacterial activities

2.4.1. Culture of bacterial strains

The bacterial strains used were *Staphylococcus aureus* (NCTC® 10788) (SA1), *Staphylococcus aureus* (ATCC® BAA1707TM) (SA2), *Pseudomonas aeruginosa* (ATCC® 9027) (PA1) and *Pseudomonas aeruginosa* [PAO1] (ATCC®BAA- 47) (PA2). All the strains were obtained from LGC Standards, Middlesex, UK, maintained at 4˚C and sub-cultured at regular intervals on fresh media. Prior to each antibacterial study, the bacterial strains were cultivated in tryptic soy broth (TSB), at 100 rpm and 37˚C overnight. The bacterial pellets were collected by centrifugation for 25 minutes at 3000 rpm. The formed pellet was resuspended in fresh TSB and optical density at 550 nm of the bacterial suspensions was set in order to obtain an equivalent to 1.5×10^8 CFU/mL.

2.4.2. Determination of minimum inhibitory concentration and minimum bactericidal concentration

The minimal inhibitory concentrations (MIC) and minimal bactericidal concentrations (MBC) of DOX, blank NPs and DOX-loaded NPs were determined by a microtiter broth dilution technique in 96-well bottom-plates as per the protocol of the Clinical and Laboratory Standards Institute (Patel J.B. et al., 2015). Briefly, 100 µL bacteria suspension (1.5×10^8 CFU/mL) was cultured in a 96-well plate in their respective medium in the presence of 100 µL of different concentrations of DOX, blank NPs and DOX-loaded NPs, resulting in 2×10^5 CFU/mL of bacteria. The microplates were incubated at 37 °C for 24 h. The MIC was defined as the lowest concentration of DOX, blank NPs and DOX-loaded NPs at which no visible growth of the bacteria following incubation was observed. For MBC determination, 20 µL from wells corresponding to the MIC and the above-mentioned dilutions were cultured onto TSA plates and incubated at 37˚C for 24 hours. Afterwards, the bacterial colonies on the plates were counted. The lowest concentration that killed 99.9% of the bacterial growth was defined as the MBC.

232 *2.4.3. Time kill assay*

233 Time-killing kinetics of DOX and DOX-loaded NPs against SA and PA were determined as per
234 the method described previously (Chen et al., 2018). In brief, concentrations equal to MIC, 2 x
235 MICs and 4 x MICs of DOX, blank NPs and DOX-loaded NPs were prepared and were added into
236 the bacterial suspensions, resulting in 2×10^5 CFU/mL of bacteria. The bacterial cultures were
237 then incubated at 37˚C. Aliquots of 20 µL from the cultures were collected at time intervals of 0,
238 2, 4, 6, 8, 12, 18 and 24 h and inoculated aseptically into TSA plates. The plates were incubated at
239 37°C for 24 h and the viable colony forming units (CFU) of the bacteria was determined. The
240 procedure was carried out in triplicate and a curve of the log CFU/mL was constructed against
241 time-kill.

242

243 *2.5. In-vitro release study of DOX-loaded NPs in bacterial cultures*

244 The release studies of free DOX and DOX-loaded NPs were carried out with or without the
245 bacterial cultures (Xiong et al., 2012). Briefly, NPs equivalent to 5 mg of DOX were dispersed in
246 5 mL of the bacterial cultures (optical density at 550 nm was set to 0.1) and were incubated in an
247 orbital shaker at 100 rpm, 37°C. At predetermined time intervals, aliquots of 0.5 mL of sample
248 were drawn out and were filtered using Amicon® Ultra Centrifugal Device (Millipore Inc,
249 molecular weight cut-off (MWCO) of 12 kDa). The amount of DOX in the filtrate was quantified
250 by HPLC. Following this, common mathematical kinetic models, namely zero order, first order,
251 Higuchi, Korsmeyer-Peppas and Hixson-Crowell were applied to the cumulative DOX released
252 (Permana et al., 2019c). DDsolver (China Pharmaceutical University, Nanjing, China) was used
253 to determine the model parameters (Zhang et al., 2010b).

254

2.6. In vitro antibiofilm activities

2.6.1 96-Well Microtiter Plate (MTP) Biofilm Study

The effects of DOX, blank NPs and DOX-loaded NPs on biofilm-grown of SA and PA were carried out using the crystal violet technique (Bazargani and Rohloff, 2016). Briefly, these bacterial cells were cultivated in TSB with 3% (w/v) NaCl and 0.5% (w/v) glucose (TSB-NG) and diluted to obtain 2×10^5 CFU/mL of bacteria. Aliquots of 200 µL of the bacterial suspension were then placed into a 96-well plate and were incubated for 24 h at 37°C. Afterwards, the wells were carefully washed thrice with sterile PBS to remove any non-adherent microorganisms. The concentrations equal to MIC, 2 x MICs and 4 x MICs of DOX, blank NPs and DOX-loaded NPs (200 µL), as well as TSB-NG (200 µL) as control were then added into the preformed biofilms and were incubated for 24 h at 37°C. Following incubation, the non-adherent bacterial cells were removed. The biofilms were rinsed thrice with 200 µL of sterile PBS. The plates were dried for 1 h at 25°C. The biofilm in the wells were further stained with 200 µl of 1% w/v crystal violet and were incubated for 15 at room temperature. To remove any unabsorbed stains, the wells were washed three times with sterile distilled water. An aliquot of 200 µL of ethanol was added into the washed wells to dissolve the crystal violet. Finally, the destaining solutions were moved to a new plate and the absorbance, presenting the amount of biofilm, was determined at 595 nm using a FLUOstar Omega spectrophotometer (BMG LabTech, Ortenberg, Germany). The killing percentage was calculated using Equation (3).

$$\text{Killing percentage} = \frac{Abs_{control} - Abs_{experimental}}{Abs_{control}} \; x \; 100\% \qquad \text{Equation (3)}$$

2.6.2. Colony Biofilm Model (CBM)

The antibiofilm activities of DOX, blank NPs and DOX-loaded NPs were also evaluated in the CBM (Alhusein et al., 2016), with slight modifications. Briefly, 50 µL of the diluted bacterial 2 ×

10^5 CFU/mL were inoculated onto sterile 10 mm poly(carbonate) discs located on the surface of tryptic soy agar (TSA) plates. The plates were incubated for 72 h at 37°C to permit the development of the biofilm. The discs were aseptically moved to new TSA plates every day for 4 days. Afterwards, 100 µL DOX, blank NPs and DOX-loaded NPs with the concentrations equal to MIC, 2 x MICs and 4 x MICs were spotted on to the discs using a micropipette. The disc without any treatments was used as a control. The plates were further incubated at 37°C for 24 h. Following 24 h incubation, each disc was moved to a tube containing 5 mL of TSB and were vortexed for 5 min to separate the bacteria from the discs and to disrupt the biofilms. The suspended cells were then diluted appropriately and 20 µL were inoculated aseptically into TSA plates. The plates were incubated at 37°C for 24 h and the viable CFU were calculated. The killing percentage was calculated using Equation (4).

$$\text{Killing percentage} = \frac{CFU_{control} - CFU_{experimental}}{CFU_{control}} \; x \; 100\% \qquad \text{Equation (4)}$$

2.7. Fabrication of two-layered dissolving MNs

Two-layered dissolving MNs were prepared by a two-step casting technique (Permana et al., 2019c), with slight modifications. An aqueous blend of 25% w/w of PVP (58 kDa) and 15% of PVA (31-50 kDa) was used a MNs matrix. This aqueous blend was mixed with the same amount of washed pellets of DOX-loaded NPs. Following this, 50 mg of the formulation was cast into the silicone MN moulds (needle density of 16 x 16, pyramidal needles; 850 µm height [600 µm pyramidal tip, 250 µm base column] and 300 µm width at base and 300 µm interspacing). The moulds were further placed in a positive pressure chamber and a pressure of 4 bar was applied for 2 min. The excess formulations on the mould were removed using a spatula and the formulations

were dried for 4 h at room temperature. Afterwards, an aqueous gels of 15% w/w PVP (360 kDa) and 1.5% w/w glycerol was then poured on the top of dry formulation, forming the two-layered MNs. The moulds were placed again in a positive pressure chamber and a pressure of 4 bar was applied for 15 min. The MNs were finally dried at room temperature for 48 h. In addition to MNs containing DOX-loaded NPs, MNs containing free DOX were also prepared for further studies using the same method and the same DOX concentration. The morphology of MNs were visually examined using a Leica EZ4D light microscope (Leica Microscope, Milton Keynes, UK) and scanning electron microscope (SEM) TM3030 (Hitachi, Krefeld, Germany).

2.8. Evaluation of mechanical and insertion properties of dissolving MNs

Mechanical strength of MNs was evaluated using a TA-TX2 Texture Analyzer (Stable Microsystem, Haslmere, UK), as described previously (González-Vázquez et al., 2017). The insertion capability of MNs was investigated using Parafilm®M as a validated skin-simulant artificial membrane, as described in a previous study (Larrañeta et al., 2014). Additionally, the insertion property of MNs was also investigated using an optical coherence tomography (OCT) microscope (Michelson Diagnostics Ltd., Kent, UK), as outlined in previous works (González-Vázquez et al., 2017; McCrudden et al., 2018; Permana et al., 2019a), in Parafilm® M and full-thickness neonatal porcine skin. ImageJ® (National Institute of Health, Bethesda, MD, USA) software was employed to measure the length of needles inserted.

2.9. Calculation of drug content localized to the needles

To quantify the amount of DOX in MN needles, the needles were detached cautiously from the baseplate using a scalpel and were dissolved in 5 mL distilled water. The drug amount was calculated using the same protocol as described in drug loading calculation in NPs formulation.

2.10 Investigation of the effect of MN formulation on the size and PDI of SLNs

The two-layered dissolving MNs were dissolved in distilled water. Afterwards, the size and PDI of the NPs were measured using DLS and were compared to the size and PDI of NPs before being formulated into MNs arrays.

2.11. Dissolution study, ex vivo dermatokinetic studies and antibiofilm activity in ex vivo model of biofilm on porcine skin

2.11.1. Preparation of ex vivo model of biofilm on porcine skin

Excised full-thickness skin from stillborn piglets was obtained as described previously (Permana et al., 2019a). The skins were sterilised by immersing in 70% ethanol for 1 h and were dried for 20 min in a biosafety cabinet. *Ex vivo* models of biofilm in the excised full-thickness neonatal porcine skin were created by following the methods described previously (Alhusein et al., 2016), with minor modifications. Briefly, two types of wound were created, namely using a biopsy punch (Stiefel, Middlesex, UK) and red-hot brass knob, forming cut wounds (wound 1) and burn wounds (wound 2) of diameter 5 mm, respectively. The skin pieces were aseptically placed on TSA plates in Class II Microbiological safety cabinet using a metal tweezer. Afterwards, 50 µL of the diluted bacterial suspensions 2×10^5 CFU/mL were inoculated to the wound of the skin and spread homogeneously. The plates were incubated at 37°C with the skin were aseptically transferred to

new TSA plates every day for 5 days to allow the formation of the biofilm. The biofilm formation was observed using a a Leica EZ4D light microscope and OCT.

2.11.1 Dissolution study

The MNs dissolution was considered *in situ* in *ex vivo model of biofilm on porcine skin*. Briefly, the MN arrays were then inserted into the skin section using manual pressure and a cylindrical stainless-steel weight of 5.0 g put on top to assure the array remained in the same place. At different interval time points, MN arrays were removed and viewed under a Leica EZ4 D stereo microscope.

2.11.2. Ex vivo dermatokinetic studies

Ex vivo dermatokientic studies of dissolving MNs containing free-DOX and DOX-loaded NPs were conducted in uninfected and biofilm model on excised full-thickness porcine skin. This study was carried out as per a method described previously (Permana et al., 2019a, 2019c), Initially, the skin was attached to the donor compartment of the Franz cell diffusion cells using a cyanoacrylate glue. The MNs were inserted into the skin for 30 s using manual force and the donor compartment was connected to the receiver compartment containing PBS (pH 7.4). To ensure the MNs stayed in place during the experiment, a cylindrical stainless-steel mass of 5 g was placed on top of the MNs. Parafilm®M was used to seal the donor compartment and sampling arm and the temperature of the receiver compartment was maintained at 37 ± 1 °C. The compartment was stirred at 600 rpm. At predetermined time points (0.5 h, 1 h, 2 h, 3 h, 4 h, 5 h, 6 h, 8 h, 12 h, 24 h and 48 h), the MNs were removed and the skin was rinsed thrice with sterile water. To extract the DOX released in the skin, 1.5 mL water and two stainless steel beads (5 mm diameter) were added along with the skin to Eppendorf tubes and the mixture was homogenized for 15 min at 50 Hz, using a Tissue Lyser LT (Qiagen, Ltd, Manchester, UK). The samples were then centrifuged at 14,000 rpm for 30 min and the amount of DOX in supernatant was quantified by HPLC. PKSolver (China Pharmaceutical University, Nanjing, China) (Zhang et al., 2010a) was applied in a one-

compartment open model to evaluate the dermatokinetic profiles. The maximum drug concentration in skin (Cmax), the time of maximum concentration (t_{max}), the drug concentration time curve from time zero (t = 0) to the last experimental time point (t = 72 h) (AUC), the mean half-life ($t_{1/2}$) and the mean residence time (MRT) were all determined. In order to ensure that the extraction method was only able to extract the DOX released from NPs without disrupting the NPs, the two stainless steel beads were also separated added into DOX-loaded NPs dispersion and processed as the same procedure as the skin extraction. As a comparison, needle-free patches containing free-DOX and selected DOX-loaded NPs were prepared and the same studies were carried out.

2.11.3 Antibiofilm activity in ex vivo model of biofilm on porcine skin

Antibiofilm activity was sudied using the method described previously (Alhusein et al., 2016; Roche et al., 2019), with slight modifications. To evaluate the antibiofilm activity of dissolving MNs and needle-free patches containing free-DOX and DOX-loaded NPs in *ex vivo* model, 20 µL of the supernatant collected from dermatokinetic studies following 24 h and 48 h application time were inoculated into TSA plates and were incubated for 24 h at 37°C. Additionally, blank dissolving MNs were also applied to the infected skin and the same procedure was performed. The numbers of viable CFU were finally counted. Infected skin without MNs application were used as a positive control and normal skin were used as a negative control.

2.12. Instrumentation and chromatographic condition for analytical method

The concentrations of DOX in all studies were quantified by HPLC (Agilent Technologies 1220 Infinity UK Ltd, Stockport, UK) as described earlier (Permana et al., 2019b), with slight modifications. The quantifications were performed using a Xselect CSH™ C18 column (Waters,

391 3.0 × 150 mm with particle sizes of 3.5 µm) with the flow rate of 0.4 mL/min. A mixture of
392 0.1% *v*/*v* of trifluoroacetic acid in water and acetonitrile (65:35 *v*/*v*) was used as the mobile phase
393 and UV detector was set at 270 nm. The injection volume was 25 µL and the quantification were
394 conducted at room temperature. This analytical method was validated according to the
395 International Committee on Harmonisation (ICH) guidelines 2005.
396
397 *2.13. Statistical analysis*
398 The experimental results were reported as means ± standard deviation (SD) of the mean. The
399 results were statistically analysed using GraphPad Prism® version 6 (GraphPad Software, San
400 Diego, California, USA). An unpaired t-test was used to compare two groups. The Kruskal-Wallis
401 test with post-hoc Dunn's test was used to compare multiple groups. A value $p < 0.05$ denoted
402 statistical significance.
403
404 **3. Results and Discussion**
405 *3.1. Formulation of DOX-loaded NPs*
406 DOX-loaded PLGA and PCL were prepared a using double emulsion method because this
407 method is an appropriate method to formulate NPs containing hydrophilic molecules (Cohen-Sela
408 et al., 2009), like DOX. For chitosan NPs, the formulations were prepared using the ionotropic
409 gelation between positively charged chitosan with negatively charged TPP (de Carvalho et al.,
410 2019). The characteristics of NPs are shown in Table 2. The results showed that the particle sizes
411 of NPs were found to be 247.5 ± 12.5 nm, 208.3 ± 9.8 nm, 262.6 ± 21.4 nm, 235.1 ± 11.2 nm and
412 217.4 ± 10.3 nm for NP-1, NP-2, NP-3, NP-4 and NP-5, respectively. It was observed that NPs
413 obtained from PCL (NP-2) were significantly smaller ($p < 0.05$) compared to PLGA NPs (NP-1).

It has been postulated that PCL chains possess higher flexibility than PLGA chains and, therefore, the formulation of drugs into this polymer could potentially result in smaller particle sizes (Mundargi et al., 2007). When compared to chitosan NPs (NP-5), the particle sizes of NP-1 were found to significantly greater ($p < 0.05$). This may be due to the hydrophobicity of PLGA in comparison to chitosan, which could potentially affect the particle size in NP formulations. For NP-3 and NP-4, the particle sizes were greater compared to NP-1 and NP-2 most likely because of the coating process of chitosan onto the surface of PLGA and PCL NPs. Specifically, the incorporation chitosan into PCL NPs did not increase the particle size significantly ($p > 0.05$). With respect to PDI values, it was found that the values were in the range of 0.198 ± 0.004 and 0.232 ± 0.003, demonstrating the generally homogeneous and monodispersed profile of these NPs.

Table 2. Particle size, PDI, zeta potential, encapsulation efficiency and drug loading capacity of different formulations of DOX-loaded NPs (means ± SD, $n = 3$).

Formulations	Particle size (nm)	PDI	Zeta potential (mV)	EE (%)	DL (%)
NP-1	247.5 ± 12.5	0.201 ± 0.011	-6.3 ± 0.58	50.5 ± 3.4	11.9 ± 1.2
NP-2	208.3 ± 9.8	0.198 ± 0.004	-7.2 ± 0.45	43.4 ± 4.9	15.7 ± 1.3
NP-3	262.6 ± 21.4	0.213 ± 0.013	20.4 ± 1.23	51.6 ± 5.2	9.5 ± 0.8
NP-4	235.1 ± 11.2	0.232 ± 0.003	19.2 ± 0.87	42.9 ± 4.8	12.4 ± 1.1
NP-5	207.4 ± 10.3	0.215 ± 0.009	29.5 ± 1.34	53.2 ± 4.3	11.4 ± 0.9

For zeta potential, the values were -6.3 ± 0.58 mV for NP-1, -7.2 ± 0.45 mV for NP-2, 20.4 ± 1.23 mV for NP-3, 19.2 ± 0.87 mV for NP-4 and 29.5 ± 1.34 mV for NP-5. The negative zeta potentials obtained from NP-1 and NP-2 were as a result of the presence of ionized of carboxylic group of PLGA and PCL (Öcal et al., 2014). In contrast, a positive zeta potential was achieved in

the case of NPs with chitosan. This is most likely due to the presence of positive amine groups in the chitosan (Rabea et al., 2003), leading to the positively charged NPs.

Regarding the EE, it was found that the EEs of NPs prepared from PCL (NP-2 and NP-4) were significantly smaller ($p < 0.05$) compared to PLGA NPs (NP-1 and NP-3) and chitosan NPs (NP-5). The lower EE may be due to the higher hydrophobicity nature of PCL (Badran et al., 2018) in comparison with PLGA and chitosan. Therefore, the encapsulation of DOX as a hydrophilic compound were low in this polymer. The EE values were 50.5 ± 3.4%, 43.4 ± 4.9%, 51.6 ± 5.2%, 42.9 ± 4.8% and 53.2 ± 4.3% for NP-1, NP-2, NP-3, NP-4 and NP-5, respectively. In terms of DL, the values were between 9.5 ± 0.8% and 15.7 ± 1.3%. After the attachment of chitosan to the surface of PLGA and PLGA NPs, the DLs of these NPs (NP-3 and NP-4) decreased from 11.9 ± 1.2% to 9.5 ± 0.8 and from 15.7 ± 1.3% to 12.4 ± 1.1%. This was caused by the additional amount of NPs composition, while maintaining the amount of DOX in the NPs, leading to the decreasing DL value.

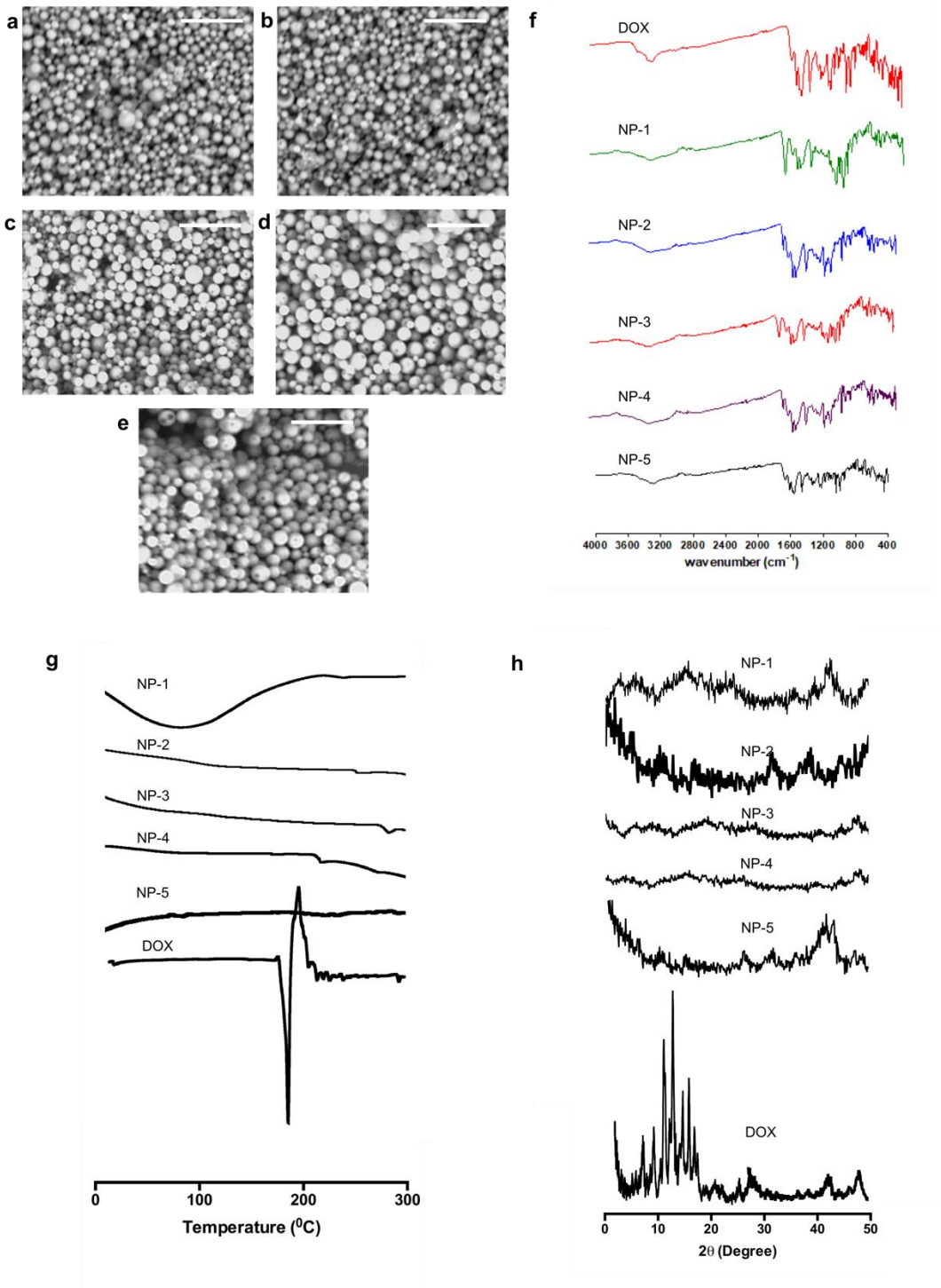

447

448 **Figure 1.** SEM images of NP-1 (**a**), NP-2 (**b**), NP-3 (**c**), NP-4 (**d**) and NP-5 (**e**) at a magnification power of 30000x
449 (The white scale bar represents a length of 1 µm in each case). FTIR spectra of DOX, NP-1, NP-2, NP-3, NP-4 and
450 NP-5 (**f**). DSC thermogram of DOX, NP-1, NP-2, NP-3, NP-4 and NP-5 (**g**). X-ray diffractogram of DOX, NP-1, NP-
451 2, NP-3, NP-4 and NP-5 (**h**)

The morphologies of DOX-loaded NPs observed by SEM are depicted in Figure 1a-1e. As shown in SEM images, all formulations were approximately spherical in shape. Importantly, the sizes obtained in this observation were in close agreement with the results obtained from DLS analysis (˜200 nm).

FTIR spectra of DOX and their respective NPs formulations are depicted in Figure 1f. The spectra indicate that DOX had a major peak at 1518 cm^{-1} due to aromatic N-H bending. Specific peaks were also observed between 1341 cm^{-1} and 1679 cm^{-1} due to aromatic C=O and C=C stretching. Peaks were found at 2921 cm^{-1}, 3311 cm^{-1} and 3432 cm^{-1} relating to C-H stretching, primary N-H group and primary O-H group, respectively. Importantly, specific groups were also observed in FTIR spectra of all NPs formulations. Accordingly, chemical interactions between excipients used and DOX were not shown to occur.

The DSC analysis results of DOX and DOX-loaded NPs are shown in Figure 1g. The results showed sharp endothermic peaks at 178°C in DOX, owing to the melting points of the DOX crystals. Nevertheless, this peak was not observed in DOX-loaded NPs. The XRD diffractograms of the pure DOX and its NP formulations are depicted in Figure 1h. Sharp characteristics peaks of DOX were observed at 2θ values of 10.42, 15.21, 17.71 and 19.98, because of high crystalline characteristics of DOX, as reported previously (Eskitoros-Togay et al., 2019). However, similar to DSC analysis results, these peaks were not observed in NP formulations. The absence DOX peak in DSC and XRD analysis may be caused by the complete encapsulation of DOX in amorphous or solution form in the NP polymers used in this study.

3.2. In vitro antibacterial activities

3.2.1. Determination of minimum inhibitory concentration and minimum bactericidal concentration

The antibacterial activity of free DOX and DOX-loaded NP formulations were further investigated. The comparison of MIC and MBC values between DOX solution and their NP formulations are presented in Table 3. The results implied that the formulation of DOX into NPs enhanced the antibacterial activity of DOX against SA and PA strains. Specifically, the NPs prepared from chitosan (NP-3, NP-4 and NP-5) exhibited lower MIC and MBC, compared to the NPs without chitosan. This was a result of the utilization of chitosan in our formulation. In the blank NPs, despite higher MIC and MBC obtained in our study, it was found that the blank NPs containing chitosan showed antimicrobial activities against all bacterial strains. Similarly, it has been well reported that chitosan has an antibacterial activity (Choi et al., 2019; Noel et al., 2010; Rabea et al., 2003). In this study, all MBC values were higher than MIC, indicating that higher DOX concentration was required to kill the bacterial cultures. Comparing the ratio of MBC to MIC, it was found that the ratio of these values in all case were < 4. The ratio of ≤ 4 is denoted as bactericidal and the ratio of > 4 is denoted as bacteriostatic (Tato et al., 2014). Accordingly, our study suggested that both DOX and DOX-loaded NPs possessed bactericidal activities.

493 **Table 3**. MIC and MBC values of free DOX, blank NPs and DOX-loaded NPs (n= 3)

		Bacterial strains							
		SA1		SA2		PA1		PA2	
		DOX-loaded NPs	Blank NPs	DOX-loaded NPs	Blank NPs	DOX-loaded NPs	Blank NPs	DOX-loaded NPs	Blank NPs
MIC (μg/mL)	Free DOX	12.5	>12800	25	>12800	25	>12800	50	>12800
	NP1	6.25	>12800	12.5	>12800	12.5	>12800	25	>12800
	NP2	6.25	>12800	12.5	>12800	12.5	>12800	25	>12800
	NP3	3.125	400	6.25	800	6.25	400	12.5	3200
	NP4	3.125	400	6.25	800	6.25	400	12.5	3200
	NP5	3.125	200	3.125	400	3.125	200	6.25	1600
MBC (μg/mL)	Free DOX	25	>12800	50	>12800	25	>12800	100	>12800
	NP1	12.5	>12800	25	>12800	25	>12800	50	>12800
	NP2	12.5	>12800	25	>12800	25	>12800	50	>12800
	NP3	6.25	800	12.5	1600	12.5	1600	25	6400
	NP4	6.25	800	12.5	1600	12.5	1600	25	6400
	NP5	6.25	400	12.5	800	6.25	800	25	3200

494

3.2.2. Time kill assay

In an attempt to explain the time required by DOX and DOX-loaded NPs to kill the bacterial strains tested, time kill assays were carried out. Figure 2a displays the time kill curve of free DOX and DOX-loaded NPs against four bacterial strains. In the untreated cohort, the viable bacterial counts increased by around 6.8 log CFU following 24 h incubation time in all bacterial strains. With respect to the concentration tested, DOX and DOX-loaded NPs with MIC values were not able to kill 99.99% of bacteria after 24 h. With 2 times the MIC values, no bacteria were counted in the case of free DOX after 24 h. Interestingly, at this concentration, 100% of bacteria were killed after 12 h for NP-1 and NP-2, after 12 h for NP-3 and NP-4 and after 6 h for NP-5. Similar results were also found in the concentration of 4 times of the MIC of NP-1 and NP-2. On the other hand, the killing time decreased to 4 h for NP-3, NP-4 and NP-5 after incubation with 4 times the MIC values. The results obtained here imply that the killing rates of DOX and DOX-loaded NPs were concentration dependently. The formulation of DOX into NPs were not only able to increase antibacterial activity, indicating by the lower MIC presented previously, but also decrease the time required to kill the bacteria.

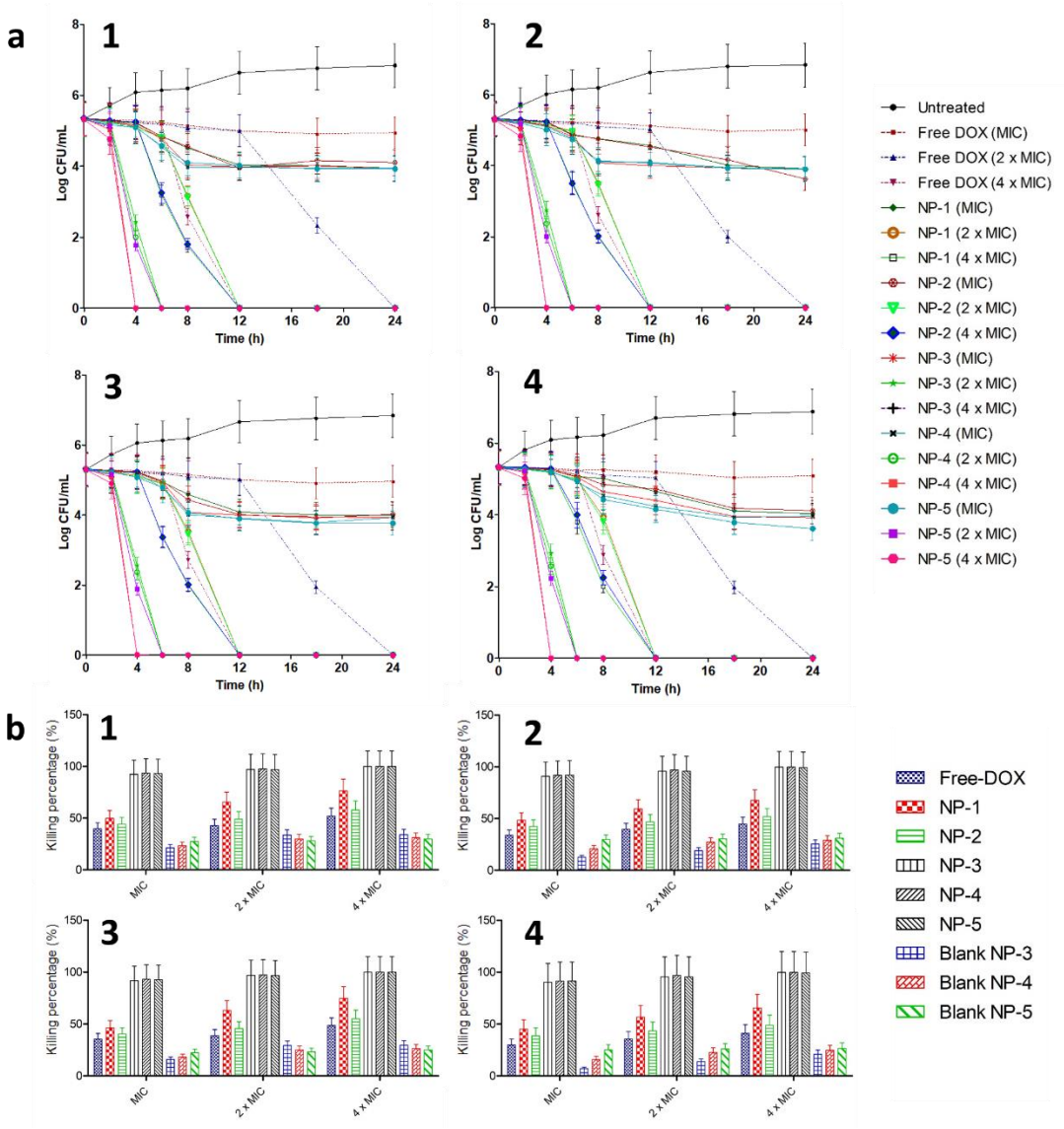

510

511 **Figure 2.** Time kill assay of DOX and DOX-loaded NPs (**a**) against *Staphylococcus aureus* (NCTC® 10788) (SA1)
512 (**1**), *Staphylococcus aureus* (ATCC® BAA1707TM) (SA2) (**2**), *Pseudomonas aeruginosa* (ATCC® 9027) (PA1) (**3**)
513 and *Pseudomonas aeruginosa* [PAO1] (ATCC®BAA- 47) (PA2) (**4**) (means ± SD, *n* = 3). Antibiofilm activity in 96-
514 well microtiter plate of DOX, DOX-loaded NPs and blank NPs (**b**) against *Staphylococcus aureus* (NCTC® 10788)
515 (SA1) (**1**), *Staphylococcus aureus* (ATCC® BAA1707TM) (SA2) (**2**), *Pseudomonas aeruginosa* (ATCC® 9027) (PA1)
516 (**3**) and *Pseudomonas aeruginosa* [PAO1] (ATCC®BAA- 47) (PA2) (**4**) (means ± SD, *n* = 3).

517
518
519
520

3.3. In vitro release study of DOX-loaded NPs in bacterial cultures

This study was designed to develop NP formulations containing DOX for specific delivery to infected site. Thus, the release behavior of DOX from its NPs formulations with and without the bacterial cultures were then investigated. Two different strains of SA and PA as above-mentioned were selected. Figure 3d depicts the cumulative percentage release of DOX from NP-1, NP-2, NP-3, NP-4 and NP5 in sterile media and media containing SA1, SA2, PA1 and P4, in comparison with DOX solution. As shown in Figure 3d, the presence of bacterial cultures significantly improved ($p < 0.05$) the release of DOX from NPs, compared to the release profiles in the absence of bacterial cultures, indicating the successful on demand delivery of these formulations. The presence of bacterial cultures did not affect ($p > 0.05$) the release behavior of DOX solutions (approximately 100% of drug released after 2 h). Specifically, after 24 h, in the absence of bacteria cultures, the release percentage of DOX were found to be 19.33 ± 1.54%, 17.03 ± 1.19%, 17.63 ± 1.41%, 14.91 ± 1.32% and 49.74 ± 3.97% from NP-1, NP-2, NP-3, NP-4 and NP-5, respectively. In the presence of SA1, 80.22 ± 5.61%, 91.06 ± 7.29%, 70.73 ± 6.98%, 83.05 ± 6.64% and 97.56 ± 8.76% of DOX were released from NP-1, NP-2, NP-3, NP-4 and NP-5, respectively. With respect to the release profile of DOX in SA2 cultures, the total release percentage of DOX were 81.96 ± 7.55% from NP-1, 93.03 ± 8.98% from NP-2, 71.79 ± 7.09% from NP-3, 84.58 ± 6.98% from NP-4 and 98.67 ± 7.98% from NP-5. In PA1 cultures, the percentages of 86.99 ± 7.93%, 98.76 ± 8.03%, 76.21 ± 7.12%, 90.06 ± 8.98% and 99.01 ± 9.82 of DOX were found to be released from NP-1, NP-2, NP-3, NP-4 and NP-5, respectively. Following 24 h incubation period with PA2, the highest percentage of DOX released from all NPs were achieved, which were 83.77 ± 5.68%, 99.43 ± 7.43%, 73.5 ± 6.98%, 94.54 ± 10.42% and 99.43 ± 7,43% from NP-1, NP-2, NP-3, NP-4 and NP-5, respectively.

The results obtained here showed the selective release profile of DOX from DOX-loaded NPs with the presence of bacterial cultures. Therefore, this approach could be potentially beneficial for permitting delivery only at the infection site, avoiding the non-specific release to uninfected areas. The difference of release behavior might be caused by the selection of polymers in the NPs formulations. It has been previously reported that, due to the rapid degradation of PCL by lipase enzymes secreted by SA, the release of vancomycin from PCL nanogels in the presence of this bacterial was significantly improved compared to the release profile without the bacteria (Xiong et al., 2012). Additionally, the release of fusidic acid from PLGA ultrafine fibers was also significantly enhanced in the presence of SA and PA (Said et al., 2011). Chitosan has been also reported to be hydrolyzed by the lipase enzyme (Chiou and Wu, 2004). Comparing the release profile of all NPs, it was shown that, despite non-significant differences ($p > 0.05$), the amount of DOX released from NP-2 was lower than NP-1 in all bacterial cultures. The higher release from NP-1 might be caused by the greater flexibility of the PCL chains compared to the PLGA chains (Badran et al., 2018), leading to the rapid hydrolysis by lipase esterase secreted by the bacterial cultures in the media. The presence of chitosan on the surface of these NPs insignificantly decreased ($p > 0.05$) the release of DOX. Hence, we successfully developed NPs laden with DOX for bacteria sensitive release.

3.4. In vitro antibiofilm activities

3.4.1. 96-Well microtiter plate (MTP) biofilm study

In burn and chronic wounds, the development of biofilm results in significant challenge in the effectiveness of antimicrobial therapy. In this study, we evaluated the ability of DOX-loaded NPs to kill the bacterial biofilms, in comparison with free DOX and blank NPs. Figure 2b exhibits the

567 percentage of reduction of bacterial biofilm after the application of DOX, DOX-loaded NPs and
568 blank NPs. For the blank NPs, as blank NP-1 and blank NP-2 did not show antimicrobial activities,
569 the antibiofilm activities of these blank NPs were not carried out. Free DOX was able to kill only
570 between 29.68 ± 3.12% and 51.75% of biofilm cells in all bacterial strains in all DOX
571 concentrations. In the concentration of four-fold of MIC, NP-1 was able to kill 76.39 ± 12.32% of
572 SA1, 67.73 ± 10.23% of SA2, 74.81 ± 11.98% of PA1 and 65.18 ± 9.34% of PA1. With respect to
573 NP-2, 57.43 ± 10.02% of SA1, 51.88 ± 8.43% of SA2, 55.02 ± 6.54% of PA1 and 48.76 ± 8.21%
574 of PA2 were killed following incubation in the concentration of four times of MIC. Interestingly,
575 in the case of NP-3, NP-4 and NP-5, more than 90% of bacterial biofilms were killed after
576 incubation in these NPs with the MIC values. More than 99% of bacterial biofilms were killed
577 when four-fold of MIC were incubated with the bacterial biofilms. In terms of the blank NPs, due
578 the presence of chitosan in the formulations, blank NP-3, blank NP-4 and blank NP-5 exhibited
579 antibiofilm activities with around 20.75 ± 3.13% - 34.03 ± 5.43% of biofilms were killed after
580 incubation in the concentration of four-fold of MIC. Analyzed statistically, NP-3, NP-4 and NP-5
581 were able to decrease the viability of bacterial biofilms significantly ($p < 0.05$) in comparison with
582 other formulations. With these results, it was observed that the presence of chitosan in the NPs
583 surface influenced the ability of NPs to kill bacterial biofilms. The presence of bacterial biofilms
584 has been reported to increase resistance of bacterial to antibacterial agents (Høiby et al., 2010). In
585 addition, conventional antibiotics have shown poor ability to penetrate bacterial biofilms. This
586 may be related to the presence of a dense barrier formed by the biofilm matrix components limiting
587 the penetration of antibiotic agents (Smith, 2005; Szomolay et al., 2005). Bacterial biofilms have
588 the net negative charge due to the presence of EPS. Therefore, the positive charge NPs might be
589 easily attached to negative charge of bacterial biofilm, enabling the penetration of antibacterial

agents into the bacterial cells (Han et al., 2017). Despite the fact that all DOX-loaded NPs were able to kill the planktonic bacteria, not all formulations showed efficacy against bacterial biofilms. We showed that only positively charged DOX-loaded NPs (NP-3, NP-4 and NP-5) exhibited effective killing percentage to the bacterial biofilms. Our results are supported by a previous study carried out by Hasan et al, reporting that positively charged clindamycin-loaded PLGA-polyethylenimine (PLGA-PEI) NPs increased the adhesion of NPs to bacteria compared to negatively charged NPs (Hasan et al., 2019). Therefore, the decoration of NPs with chitosan provides two main advantages. Firstly, the utilization of chitosan enhanced the antibiofilm activity of DOX. Secondly, the positive charge of chitosan enabled the adhesion of NPs to the bacterial biofilms.

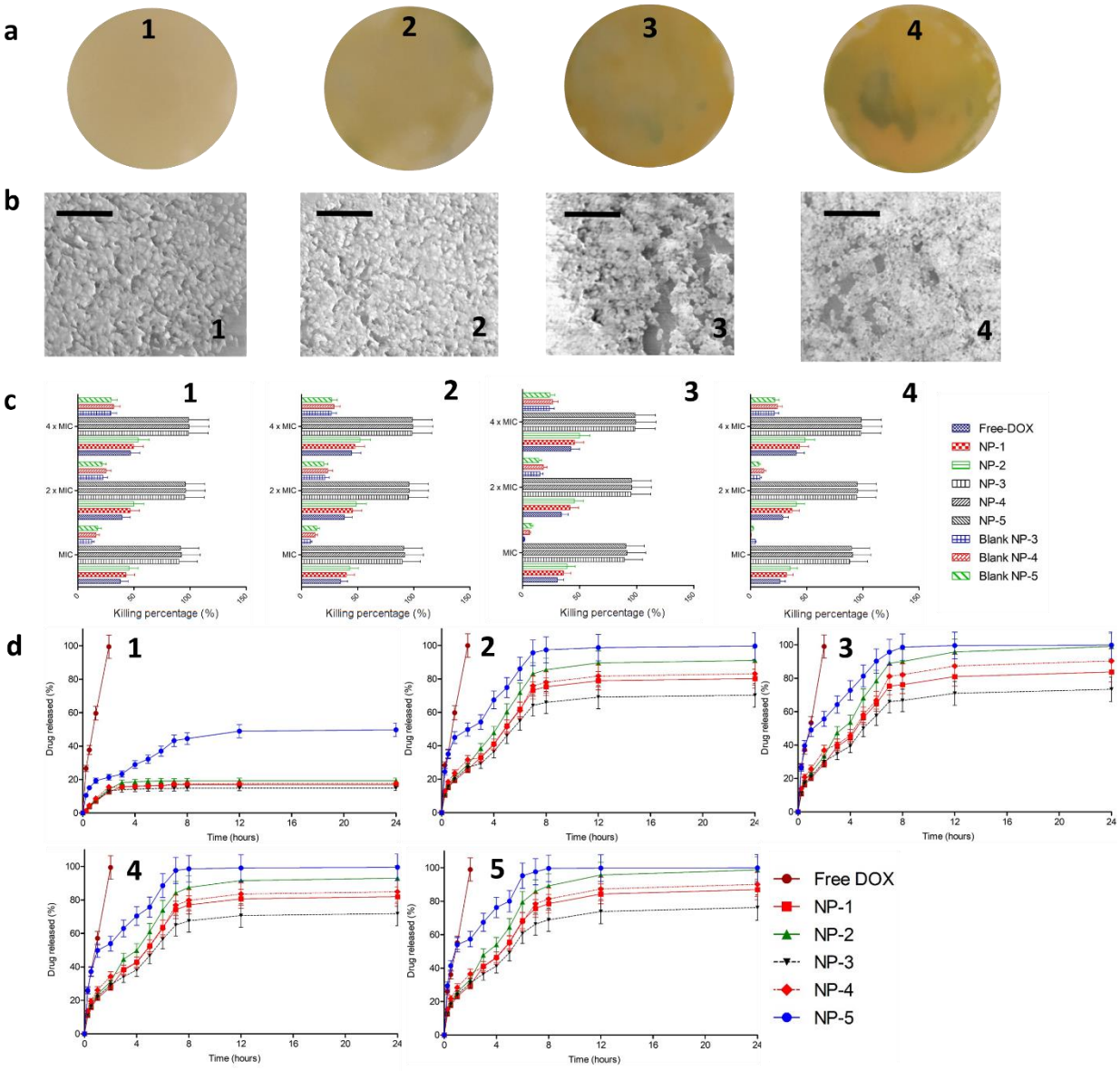

Figure 3. Representative images of colony biofilm models (CBM) (**a**) of SA1 (**1**), (SA2) (**2**), (PA1) (**3**) and (PA2) (**4**). Representative SEM images of bacterial biofilms models (**b**) of SA1 (**1**), (SA2) (**2**), (PA1) (**3**) and (PA2) (**4**) (The black scale bar represents a length of 10 µm in each case). Antibiofilm activity of DOX, DOX-loaded NPs and blank NPs in CBM (**c**) against SA1 (**1**), (SA2) (**2**), (PA1) (**3**) and (PA2) (**4**) (means ± SD, *n* = 3). *In-vitro* drug release from NPs in the absence of bacterial culture (**1**) and presence of SA1 (**2**), (SA2) (**3**), (PA1) (**4**) and (PA2) (**5**) (mean ± SD., n=3)

610 *3.4.2. Colony biofilm model (CBM)*

611 To further exploit the ability of DOX-loaded NPs to eliminate bacterial biofilms, a colony
612 biofilm model (CBM) was developed. In this model, a poly(carbonate) membrane was utilized as
613 a substrate for the growing of biofilms. The membrane was placed on top of an agar plate and the
614 mature biofilm growing in this membrane stimulates biofilm development in a wound (Alhusein
615 et al., 2016; Anderl et al., 2000). Additionally, the small fluid shear and the closeness to an air
616 boundary made by this system closely approximates the environment of wounds (Folsom et al.,
617 2011). The carbon and nitrogen source of the agar are similar to the nutrient flow in biofilms of a
618 wound (Alhusein et al., 2016). Importantly, as the membrane can be easily removed from the agar,
619 this model allows us to count the viable bacteria by resuspending the membrane in broth medium.
620 Representative images of this model are shown in Figure 3a and 3b. In this model, similar trends
621 to the MTP study were found. More 90% of bacterial biofilms were killed after 24 h incubation in
622 NP-3, NP-4 and NP-5 with MIC values (Figure 3c). More than 95% and more than 99% of bacterial
623 biofilms were killed following 24 incubation time in the concentration of two-fold and four-fold
624 of MIC, respectively. These values were significantly higher ($p < 0.05$) than the killing percentage
625 of free DOX, NP-1, NP-2 and blank NPs. Accordingly, these results showed the effectiveness of
626 PLGA and PCL NPs coated with chitosan in killing the mature bacterial biofilms.

627

628 *3.5. Fabrication of two-layered dissolving MNs*

629 After biofilm formation, an extracellular polymeric substance is produced, hampering the
630 efficient delivery of antibacterial agents. In an attempt to attain biofilm disturbance and enhance
631 the penetration of antibiotics into the biofilm, the DOX-loaded NPs were further incorporated into
632 MN arrays. The MNs were prepared using the combination of two water soluble polymers, namely

PVP and PVA. The combination of these polymers could potentially result in MNs with excellent mechanical properties, because of the hydrogen bond interaction between C = O groups of PVP and -OH groups of PVA (Permana et al., 2019c). Figure 4a and 4b show the morphology of MNs of free DOX and DOX-loaded NPs observed by light microscope and SEM. The results exhibited that all MNs produced had sharp needles. Accordingly, these formulations were further characterized for their mechanical and insertion properties.

3.6. Evaluation of mechanical and insertion properties of dissolving MNs

The MN arrays were evaluated for their mechanical strength. This evaluation was carried out to ensure the strengthen of MN arrays in resisting compression. Importantly, the capability of MNs to be inserted in the skin is a critical parameter in MNs administration, since the needle should be able to penetrate the *stratum corneum*, to release the payload in the viable skin layers. In this study, the percentage of height reduction of MN needles after the application of 32 N/MN array, equivalent to human manual compression pressure (Larrañeta et al., 2014), was calculated to determine the mechanical strength. Figure 4c depicts the mechanical properties of all formulations, represented by the percentage of reduction of MNs height. In this study, we compared these formulations with the blank MNs. The reductions in MN height were found to be 12.36 ± 3.12%, 13.03 ± 2.71%, 12.65 ± 3.22%, 12.98 ± 2.09%, 13.16 ± 3.10%, 12.91 ± 2.98% and 13.21 ± 2.11% for blank MNs, MN-free DOX, MN-NP-1, MN-NP-2, MN-NP-3, MN-NP-4 and MN-NP-5, respectively. Analyzed statistically, there were no significant differences in between the percentage of reduction of the MNs height of DOX and DOX-loaded NPs, compared to the blank MNs. As such, the formulation of DOX and DOX-loaded NPs into the dissolving MNs did not affect the mechanical properties of the dissolving MNs arrays.

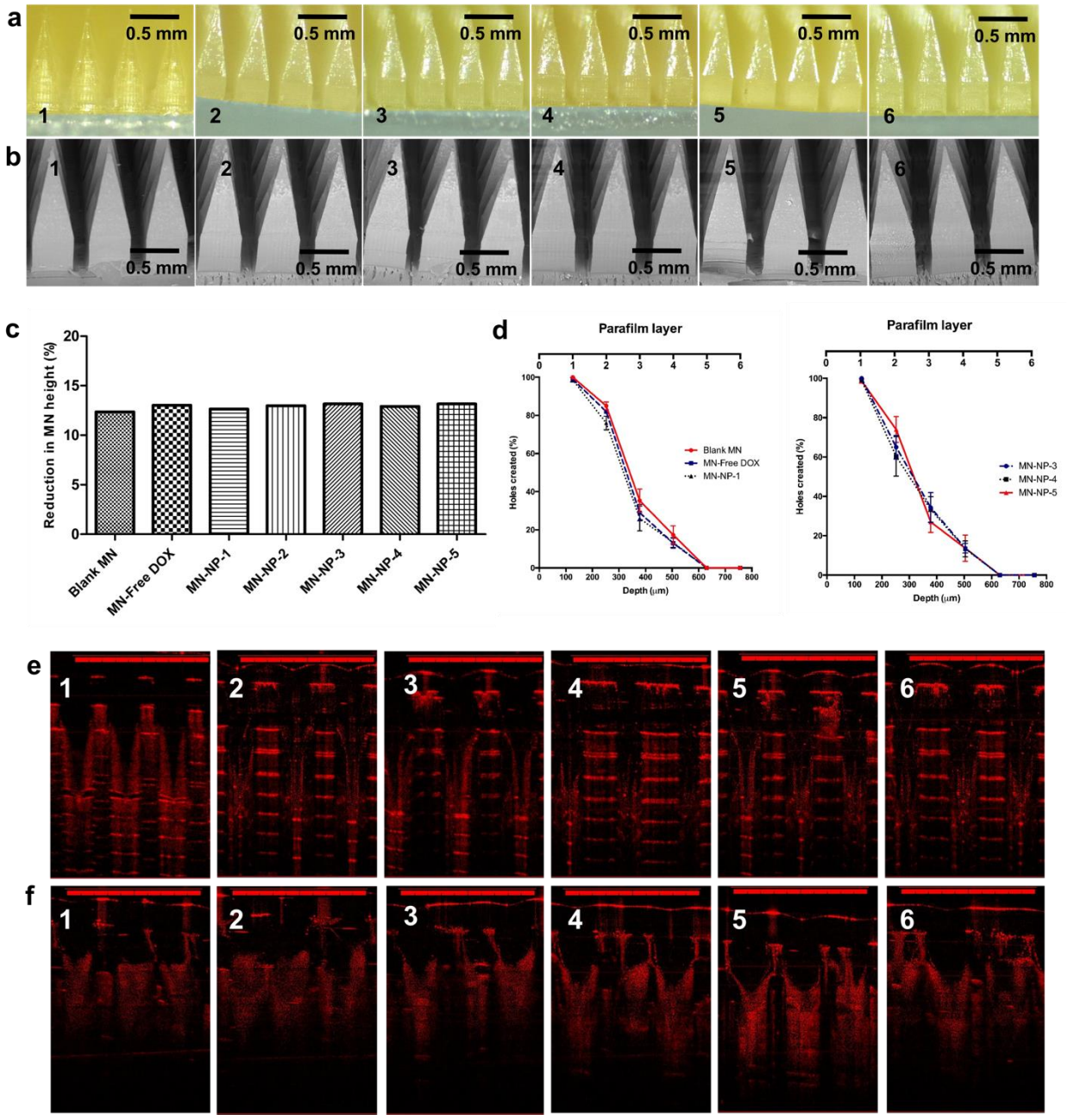

Figure 4. Light microscope images (**a**) of the MN formulations containing free DOX (**1**), NP-1 (**2**), NP-2 (**3**), NP-3 (**4**) and NP-4 (**5**) and NP-5 (**6**). SEM images (**b**) of the MNs containing free DOX (**1**), NP-1 (**2**), NP-2 (**3**), NP-3 (**4**) and NP-4 (**5**) and NP-5 (**6**). The percentage height reduction of needles on the arrays formulated containing free DOX and DOX-loaded NPs compared to blank MN arrays (means ± SD, $n = 3$) (**c**). Percentage of holes created in Parafilm®M layers, using an insertion force of 32 N/array for MN formulations containing free DOX and DOX-loaded NPs compared to blank MN arrays (means ± SD, $n = 3$) (**d**). Representative OCT images of MNs containing free DOX (**1**), NP-1 (**2**), NP-2 (**3**), NP-3 (**4**) and NP-4 (**5**) and NP-5 (**6**) following insertion into Parafilm®M film (**e**). Representative OCT images of MNs containing free DOX (**1**), NP-1 (**2**), NP-2 (**3**), NP-3 (**4**) and NP-4 (**5**) and NP-5 (**6**) following insertion into full-thickness porcine skin (**f**). The scale bar represents a length of 1 mm in each case.

For the insertion properties, eight-layers of Parafilm®M were utilized as a skin stimulant. This model has been previously validated to mimic human skin for MN insertion studies (Larrañeta et al., 2014). The result of this study is presented in Figure 4d. Similar to the mechanical properties, the formulation of DOX and DOX-loaded NPs did not affect ($p > 0.05$) the insertion properties of any of the MNs, when compared to blank MNs. The MN arrays were able to penetrate four layers of Parafilm®M. As the mean thickness of each layer of Parafilm®M is 126 µm, then the MNs were inserted up to 504 µm, indicating that around 53.9% of the needle lengths were successfully inserted. Additionally, in an attempt to envisage the profile of insertion of the MNs, optical coherence tomography (OCT) was then utilized using the Parafilm®M and the full-thickness neonatal porcine skin models. This technique has been successfully used to visualize the insertion of ability of numerous MN formulations (Donnelly et al., 2014, 2010; González-Vázquez et al., 2017; Lutton et al., 2015; McCrudden et al., 2014; Vora et al., 2018). Figure 4d and 4f depict the OCT visualization of the MNs insertion into the Parafilm®M and the full-thickness neonatal porcine skin, respectively. Analyzed using ImageJ®, the penetration depth of MNs into Parafilm®M were recorded to be 502.12 ± 21.32 µm for blank MN, 498.98 ± 19.32 µm for MN-free DOX, 505.87 ± 33.09 µm for MN-NP-1, 504.02 ± 14.54 µm for MN-NP-2, 501.16 ± 22.18 µm for MN-NP-3, 506.98 ± 29 µm for MN-NP-4 and 500.65 ± 20.32 µm for MN-NP-5. In the full-thickness porcine skin, the penetration depth of 503.65 ± 12.43 µm, 500.43 ± 10.12 µm, 506.43 ± 21.11 µm, 498.43 ± 10.41 µm, 502.11 ± 10.03 µm and 499.87 ± 10.03 µm for blank MN, MN-free DOX, MN-NP-1, MN-NP-2, MN-NP-3, MN-NP-4 and MN-NP-5, respectively. These values were in close agreement with those obtained in the insertion study according to percentages of holes created. Analyzed statistically, there were no significant differences ($p > 0.05$) in the

689 penetration depth of all MNs. Hence, the incorporation of DOX and DOX-loaded NPs into
690 dissolving MNs did not alter the penetration ability of MN arrays.
691
692 *3.7. Calculation of drug content localized to the needles*
693 After drying, the amount of DOX located in each MN array was determined to be 0.81 ± 0.09
694 mg for MN-NP-1, 1.08 ± 0.11 for MN-NP-2, 0.82 ± 0.04 mg for MN-NP-3, 1.04 ± 0.08 mg for
695 MN-NP-4 and 0.83 ± 0.05 mg for MN-NP-5. Accordingly, these drug amounts reflected the dosage
696 of DOX in one MN array in the subsequent studies.
697
698 *3.8. Investigation of the effect of MN formulation on the size and PDI of SLNs*
699 One of the critical parameters in the formulation of NPs into dissolving MNs is the ability of the
700 formulations to maintain the NP characteristics, specifically their sizes, PDIs and zeta potentials.
701 Table 4 exhibits the NP properties in the MN formulations. These findings suggest that the
702 incorporation NPs into MN arrays did not significantly ($p > 0.05$) affect the size, PDI and zeta
703 potential of DOX-loaded NPs.
704
705 **Table 4.** Particle size, PDI and zeta potential of different formulations of DOX-loaded NPs in MN formulations
706 (means ± SD, $n = 3$).

Formulations	Particle size (nm)	PDI	Zeta potential (mV)
NP-1	251.3 ± 11.3	0.223 ± 0.017	-5.6 ± 0.56
NP-2	211.6 ± 10.2	0.187 ± 0.013	-6.5 ± 0.98
NP-3	232.1 ± 19.3	0.205 ± 0.017	19.9 ± 1.87
NP-4	247.4 ± 12.7	0.214 ± 0.002	20.6 ± 2.02
NP-5	251.8 ± 9.1	0.221 ± 0.014	27.3 ± 1.72

707

3.9. Ex vivo dermatokinetic studies and antibiofilm activity in ex vivo model of biofilm on porcine skin

To further understand the release kinetic profile of DOX from NPs in the dissolving MNs, a dermatokinetic study was performed in normal full-thickness porcine skin and *ex vivo* model of biofilm on the full-thickness porcine skin. Initially, *ex vivo* model of biofilm on full-thickness porcine skin was developed. This skin models are depicted in Figure 5a. Dissolution studies of MN formulations containing drug-loaded NPs were investigated, with a view to predicting the time required for the needles to be dissolved in the skin during application. As shown in Figure S1, dissolution of MNs while in place in the skin was reached by 20 min, with needles dissolved and a reduction in height obvious after 5 min. In addition, the models were also observed using OCT (Figure 5b). The results showed that the normal neonatal porcine skin exhibited smooth surface and *ex vivo* model of biofilm wound exhibited uneven surface of the skin. OCT method has shown its effectiveness for cross-sectional observations of bacterial biofilm (Mohan et al., 2019). In order to ensure that the release of DOX was affected by the presence of bacterial biofilms, we quantified only the DOX released from NPs. For this purpose, the skin samples were homogenized at each time interval using water as solvent. This method was also applied to NP dispersions to evaluate whether this method could disrupt the NPs. Our results showed that no DOX was detected in the supernatant of NP dispersions, showing that this method would only extract DOX released from NPs. This study was carried out in two types of biofilm model, namely cut wound biofilm (wound 1) and burn wound biofilm (wound 2). Four bacterial strains mentioned previously were used to form the biofilms. Figures 5c and 6 illustrate the kinetic profiles of DOX in the non-infected skin and the *ex vivo* biofilm models, presented as the concentration versus the time of application, following the application of the MNs laden with five different DOX-loaded

NPs formulations. We further analyzed the dermatokinetic profiles of DOX, namely C_{max}, T_{max}, $T_{1/2}$, AUC and MRT, in these different formulations. The detail of the dermatokinetic profiles of DOX following the administration of the MN-free DOX and the MN-NPs laden with DOX are shown in Table S1-S5. In the non-infected skin, the release of DOX from the nanoparticles was negligible as compared to the free DOX, implying that the NPs could potentially avoid the non-specific release of DOX. Instead, in both biofilm models created from all bacterial strains, the release of DOX was significantly enhanced ($p < 0.05$) by the using of PLGA, PCL and chitosan in NP formulations. Specifically, despite non-significant difference ($p > 0.05$), the value of C_{max} of DOX from MN-NP-1, MN-NP-2 and MN-NP-5 were lower as compared to MN-NP-3 and MN-NP-4, respectively.

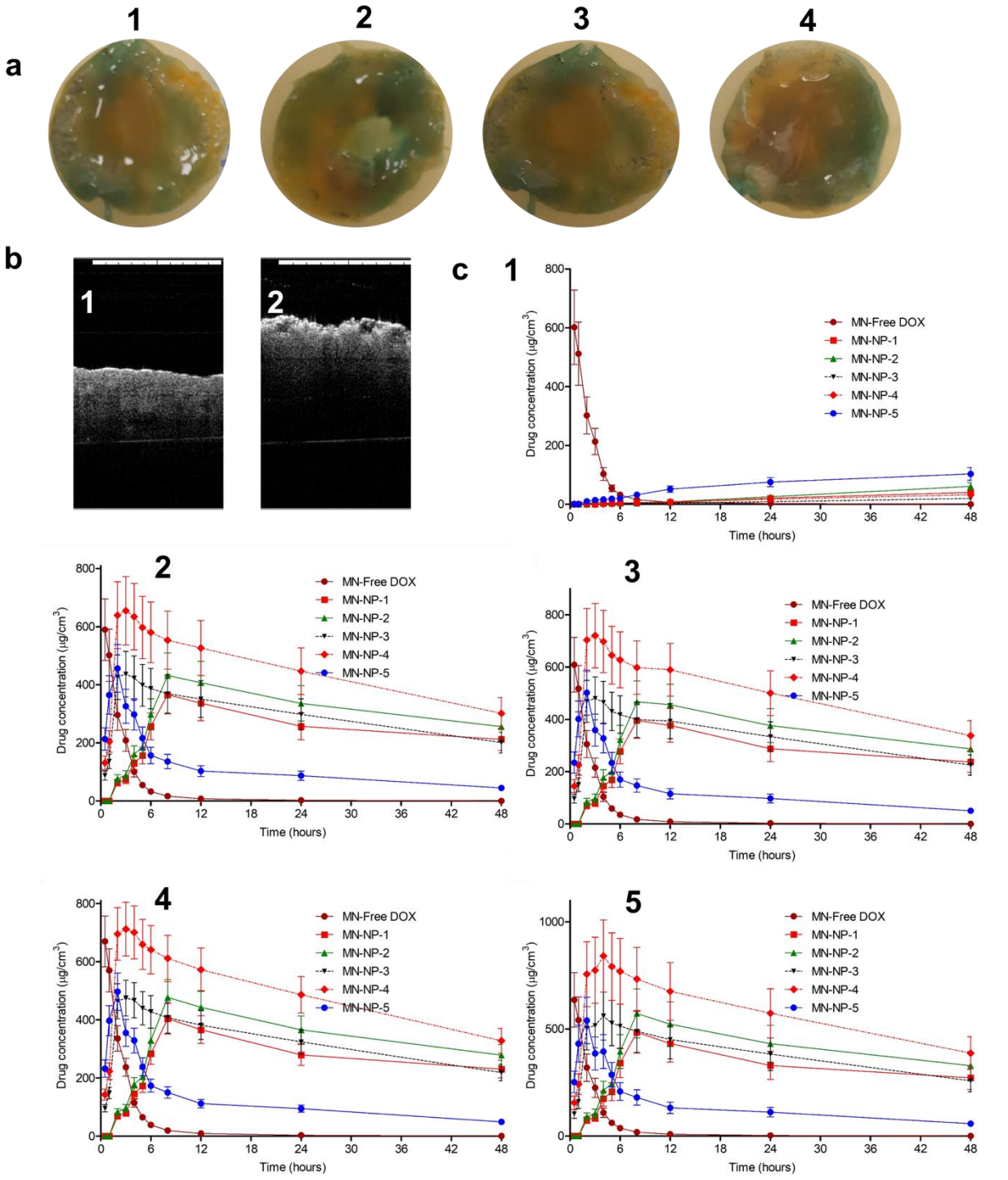

741

742 **Figure 5.** Representative images of *ex vivo* model of biofilm on full-thickness porcine skin (**a**) of SA1 (**1**), (SA2)
743 (**2**), (PA1) (**3**) and (PA2) (**4**). OCT images of normal skin and *ex vvo* model of biofilm on porcine skin (**b**). The *ex*
744 *vivo* DOX concentrations and time profiles (**c**) in non-infected full-thickness neonatal porcine (**1**), as well as *ex vivo*
745 biofilm model in wound-1 (cut wound) formed by SA1 (**2**), SA2 (**3**), PA1 (**4**) and PA2 (**5**), following the application
746 of MN containing free DOX and DOX-loaded NPs (means ± S.D., $n = 3$).

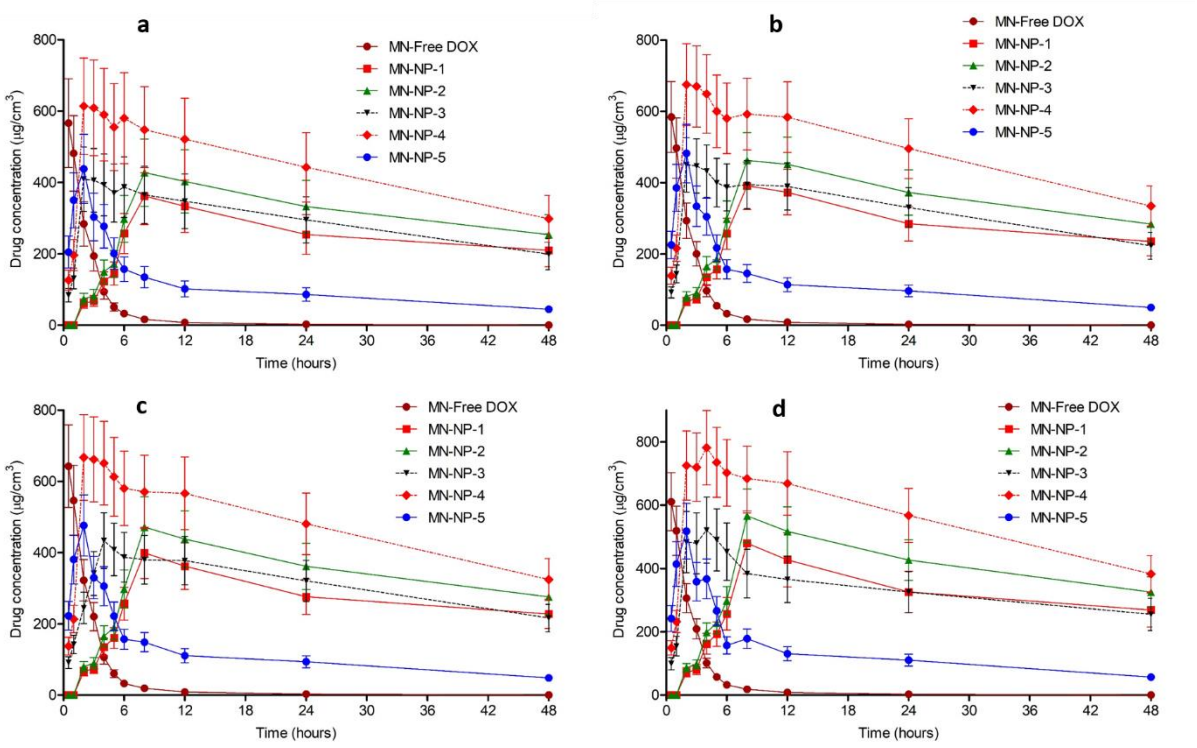

747

748 **Figure 6.** The *ex vivo* DOX concentrations and time profiles in *ex vivo* biofilm model in wound-2 (burn wound)
749 formed by SA1 (**a**), SA2 (**b**), PA1 (**c**) and PA2 (**d**), following the application of MN containing free DOX and DOX-
750 loaded NPs (means ± S.D., $n = 3$). (means ± S.D., $n = 3$).

751

752 The findings achieved here suggest that the encapsulation DOX in PLGA and PLC NPs coated
753 chitosan could increase the concentration of DOX by two possible mechanisms. Initially, the outer
754 layer of chitosan helped the NPs to be attached to the biofilm. Following this, the presence of
755 lipase secreted by the bacterial strains degraded PLGA and PCL layers, leading to the release of
756 DOX from NPs. With respect to T_{max}, due to the reasons explained for the C_{max} results, the T_{max}
757 values of DOX from MN-NP-3 and MN-NP-4 were found to be significantly lower ($p < 0.05$)
758 compared to other NP formulations. In terms of the retention time in the skin, it was found that the
759 MN containing free DOX showed MRT less than 3 h. Interestingly, the MRT values of DOX from
760 MN-NPs were significantly greater ($p < 0.05$) than those in free DOX. This could be beneficial to
761 reduce the application time of DOX in infected skin using this novel combinatorial approach,

762 leading to patient acceptability of this device. In addition to this, we also performed the
763 dermatokinetic studies for needle-free patches containing DOX and DOX-loaded NPs (Figure 7).
764 In this study, due to the higher DOX release from NP-3 and NP-4, only these NP formulations
765 were selected as comparisons. The kinetic profiles of DOX from the patches are exhibited in Figure
766 8. The results showed that, without MNs, NPs were not able to disrupt and penetrate the biofilms
767 to release DOX, indicated by the significantly lower ($p < 0.05$) of DOX in all formulations
768 delivered by the needle-free patches. Accordingly, the successful delivery of DOX into *ex vivo*
769 biofilm model was a result of the combination of MN arrays and NPs.

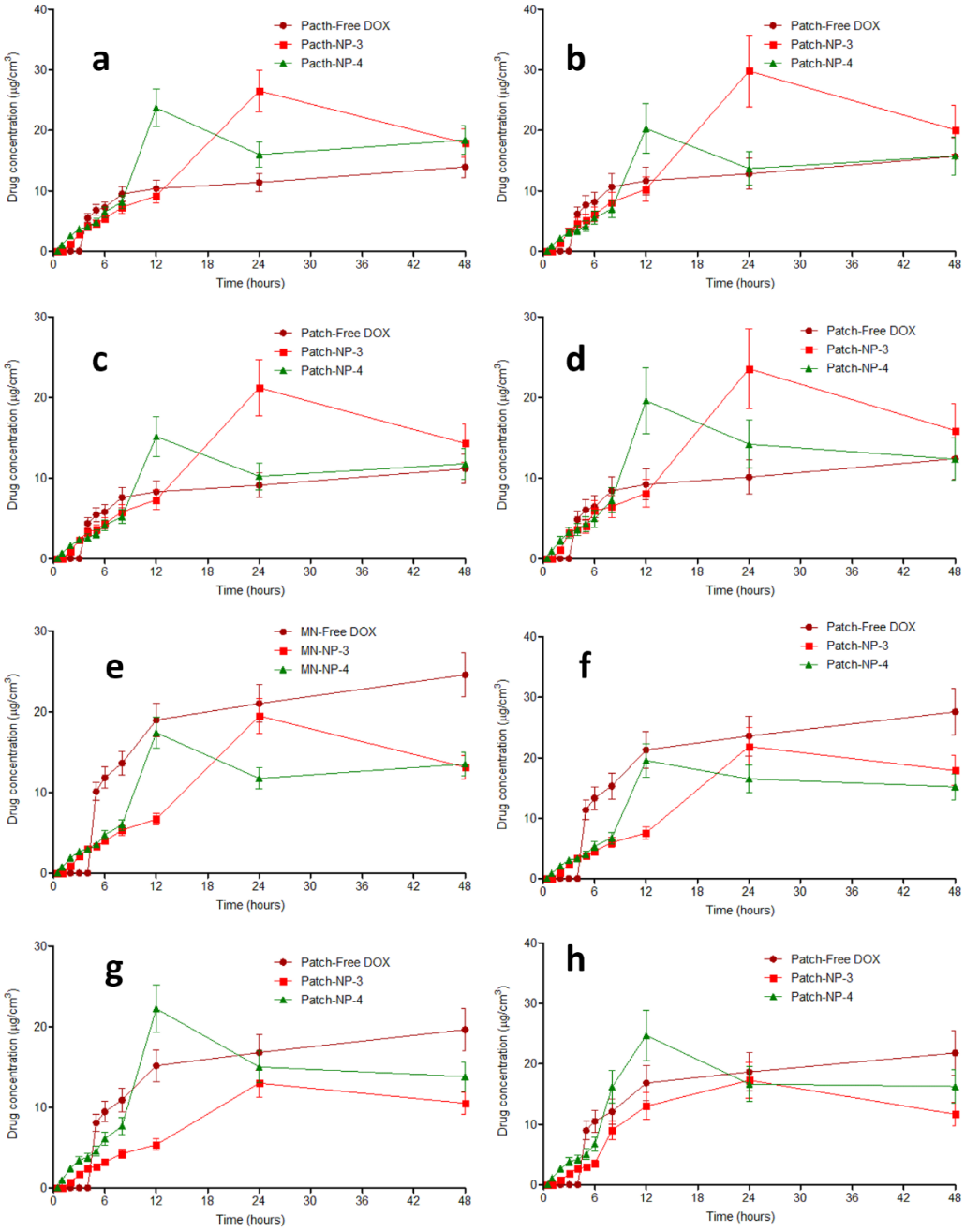

Figure 7. The *ex vivo* DOX concentrations and time profiles (**b**) in *ex vivo* biofilm model in wound-1 (cut wound) formed by SA1 (**a**), SA2 (**b**), PA1 (**c**) and PA2 (**d**), as well as *ex vivo* biofilm model in wound-2 (burn wound) formed by SA1 (**e**), SA2 (**f**), PA1 (**g**) and PA2 (**h**) following the application of needle-free patch containing free DOX and DOX-loaded NPs (means ± S.D., $n = 3$). (means ± S.D., $n = 3$).

Finally, to prove the efficacy of this delivery system, we evaluated the bacterial burden in an *ex vivo* biofilm models by viable cell counts. As depicted in Figure 9, after the application of the

778 blank MNs, the bacterial burden on biofilm wound models did not decrease following 48 h
779 application time. On the other hand, the bacterial viabilities were reduced following 48 h of
780 administration of MNs of DOX and DOX-loaded NPs (Figure 8). In the case of the MN-free DOX,
781 although the C_{max} was higher than MBC of DOX to all bacterial strains, the retention time of DOX
782 after its administration was lower than time required by DOX to completely kill the bacterial.
783 Therefore, the bacterial burdens of all strains after the administration of MN-free DOX were
784 reduced up to only ˜50%. With respect to MN-NP-1, MN-NP-2 and MN-NP-5, the killing rates
785 were determined to be between 70% and 80%. Importantly, due to the better dermatokinetic
786 profiles of these MNs compared to other formulations, more than 90% of bacterial burdens were
787 killed after 48 h of the administration of MN-NP-3 and MN-NP-4. Specifically, ˜99.99% of SA1
788 and PA1 and ˜97% of SA2 and PA2 were killed in both biofilm models. In the control patches
789 treatment, only around 60% of bacterial burden were reduced after 48 h treatment (Figure 9). Our
790 study is supported by Özcan et al (2013), comparing the skin retention of betamethasone valerate
791 from PLGA and chitosan NPs. It was found that the concentration of this drug in dermis following
792 the application of PLGA NPs was around 4-times higher in comparison with chitosan NPs (Özcan
793 et al., 2013). Therefore, these findings indicate that the combination of chitosan with PLGA and
794 PCL in NPs could potentially improve not only dermatokinetic profiles of DOX, but also
795 significantly enhance the efficacy of this system in *ex vivo* biofilm model in porcine skin by
796 penetrating the biofilm in the infected skin and killing the bacteria.

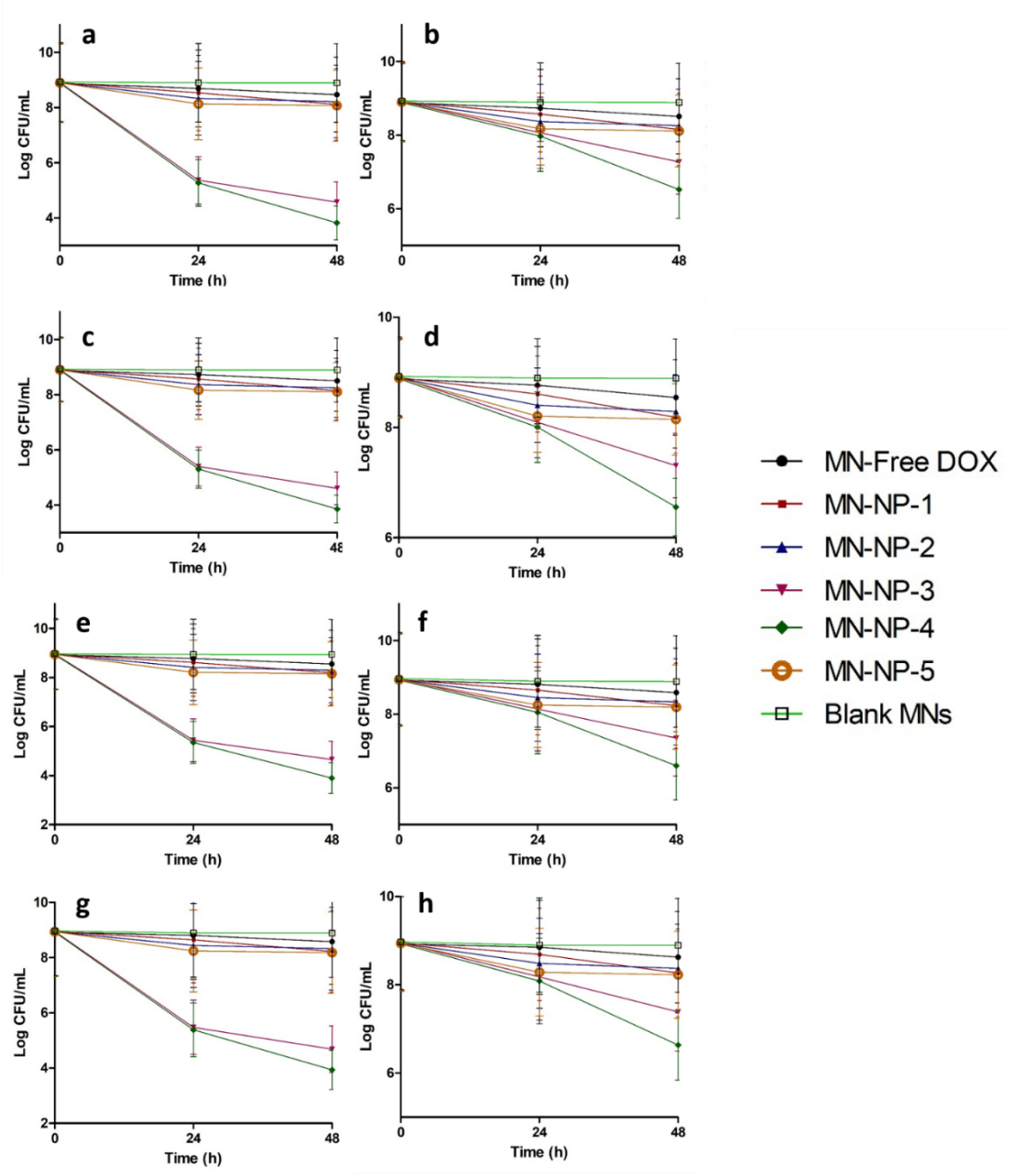

797

798 **Figure 8**. Bacterial viability (log CFU/mL) on in *ex vivo* biofilm model in wound-1 (cut wound) formed by SA1 (**a**),
799 SA2 (**b**), PA1 (**c**) and PA2 (**d**), as well as biofilm *ex vivo* model in wound-2 (burn wound) formed by SA1 (**e**), SA2
800 (**f**), PA1 (**g**) and PA2 (**h**) following the application of blank MN and MN containing free DOX and DOX-loaded NPs
801 (means ± S.D., $n = 3$). At 24 h and 48 h post-application, *ex vivo* infected skin with biofilm were homogenized in
802 sterile water and cultured onto TSA at 37 °C overnight.

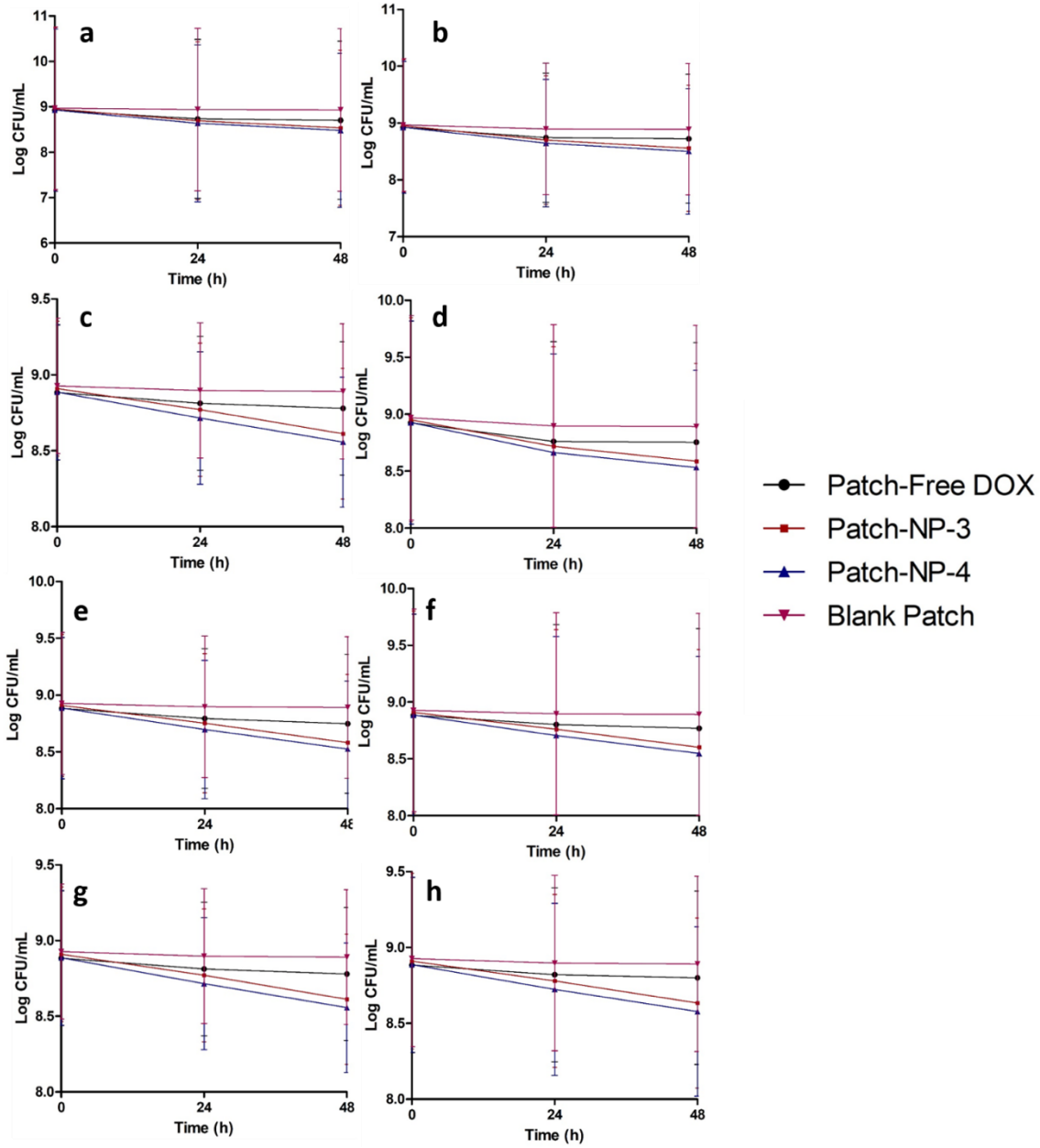

Figure 9. Bacterial viability (log CFU/mL) on in *ex vivo* biofilm model in wound-1 (cut wound) formed by SA1 (**a**), SA2 (**b**), PA1 (**c**) and PA2 (**d**), as well as biofilm *ex vivo* model in wound-2 (burn wound) formed by SA1 (**e**), SA2 (**f**), PA1 (**g**) and PA2 (**h**) following the application of blank patch and needle-free patch containing free DOX and DOX-loaded NPs (means ± S.D., $n = 3$). At 24 h and 48 h post-application, *ex vivo* infected skin with biofilm were homogenized in sterile water and cultured onto TSA at 37 °C overnight.

Taken together, the findings presented here indicate that the decoration of PLGA and PCL NPs with chitosan could result in the specific delivery of DOX in the presence of bacterial cultures. Not only that, combined with dissolving MN arrays, but this unique approach also improved the

penetration ability into bacterial biofilms in *ex vivo* biofilm models, indicated by the dermatokinetic profiles of DOX and the high bacterial burden reductions. The overriding advantage of the facilitated delivery system we have presented here, in comparison with needle-free patches, lies in the ability for site-specific delivery and long retention time in the infected skin which could potentially increase the effectiveness of antibacterial therapy of burns and chronic wounds. Following on from these promising findings, further studies are now required. Importantly, toxicity studies and *in vivo* efficacies study in a suitable infection animal models should also be carried out to completely exploit the potential applications of this system.

4. Conclusion

This study investigated the unique combination approach of bacterially sensitive NPs with dissolving MN arrays to enhance the antibiofilm properties of DOX. In NP preparations, PLGA and PCL were chosen as bacterially sensitive polymers coated with chitosan to improve the adhesion with bacterial biofilms. The NPs were spherical in shape with sizes around 200 nm. The formulation of DOX into PLGA and PCL NPs coated chitosan was able to enhance its antimicrobial and antibiofilm activity, compared to NPs prepared from only PLGA, PCL and chitosan. Furthermore, the release of DOX from the NPs was significantly affected by the presence of bacterial cultures, indicating the successful specific delivery of this system. Importantly, the incorporation of these NPs into MN arrays prepared from the combination of PVP and PVA resulted in MNs with sufficient mechanical properties and insertion abilities. Dermatokinetic studies indicated that the MNs was able improve the ability of NPs to penetrate bacterial biofilms in two *ex vivo* biofilm model in full-thickness porcine skin, namely biofilm of a burn wound and a cut wound, compared to a needle-free patch. Finally, the combination approach of PLGA and

PCL NPs coated with chitosan with dissolving MNs showed proof of principle for the successful antibiofilm activity in *ex vivo* biofilm models, indicated by the reduction of bacterial bioburden >97%. However, further comprehensive studies are warranted, including toxicity studies and *in vivo* pharmacodynamic studies in a suitable infection animal model. In conclusion, before this delivery system can reach clinical practice and attain patient benefit, acceptability and usability investigations should also be performed to confirm maximum effect of the work.

Supporting Information.

A PDF containing details on kinetic modelling of DOX release from NP formulations in the presence of *Staphylococcus aureus* (NCTC® 10788), *Staphylococcus aureus* (ATCC® BAA1707TM), *Pseudomonas aeruginosa* (ATCC® 9027) and *Pseudomonas aeruginosa* [PAO1] (ATCC®BAA- 47); and *ex vivo* dermatokinetic parameters of DOX following the administration of the MN-free DOX and the MN-NPs laden with DOX in normal excised full thickness porcine skin and *ex vivo* model of biofilm on full-thickness porcine skin are available free of charge via the Internet at http://pubs.acs.org

Author Contributions

A.D.P and R.F.D conceived the research and design of all experiments. A.D.P, M. M and E.U performed the experiment. A.D.P wrote the manuscript. M. M and E.U helped with data analysis. A.D.P wrote the manuscript. R.F.D supervised the experiment and reviewed the manuscript thoroughly. All authors have given agreement to the final version of the manuscript.

Acknowledgments

This work was supported by The Indonesian Endowment Fund for Education (Lembaga Pengelola Dana Pendidikan/LPDP). This study was alsosupported in part by Wellcome Trust grant number WT094085MA.

References

Adhirajan, N., Shanmugasundaram, N., Shanmuganathan, S., Babu, M., 2009. Collagen-based wound dressing for doxycycline delivery: in-vivo evaluation in an infected excisional wound model in rats. J. Pharm. Pharmacol. 61, 1617–1623.

Alhusein, N., Blagbrough, I.S., Beeton, M.L., Bolhuis, A., De Bank, P.A., 2016. Electrospun Zein/PCL fibrous matrices release tetracycline in a controlled manner, killing Staphylococcus aureus both in biofilms and ex vivo on pig skin, and are compatible with human skin cells. Pharm. Res. 33, 237–246.

Allen, T.M., Cullis, P.R., 2004. Drug delivery systems: Entering the mainstream. Drug Discov. 303, 1818–1822. https://doi.org/10.1126/science.1095833

Anderl, J.N., Franklin, M.J., Stewart, P.S., 2000. Role of antibiotic penetration limitation in Klebsiella pneumoniae biofilm resistance to ampicillin and ciprofloxacin. Antimicrob. Agents Chemother. 44, 1818–1824.

Badran, M.M., Alomrani, A.H., Harisa, G.I., Ashour, A.E., Kumar, A., Yassin, A.E., 2018. Novel docetaxel chitosan-coated PLGA/PCL nanoparticles with magnified cytotoxicity and bioavailability. Biomed. Pharmacother. 106, 1461–1468.

Bazargani, M.M., Rohloff, J., 2016. Antibiofilm activity of essential oils and plant extracts against Staphylococcus aureus and Escherichia coli biofilms. Food Control 61, 156–164.

882 Bharambe, S. V., Darekar, A.B., Saudagar, R.B., 2013. Wound healing dressings and drug
883 delivery systems: A review. Int. J. Pharm. Technol. 5, 2764–2786.
884 Caffarel-Salvador, E., Kearney, M.C., Mairs, R., Gallo, L., Stewart, S.A., Brady, A.J., Donnelly,
885 R.F., 2015. Methylene blue-loaded dissolving microneedles: Potential use in photodynamic
886 antimicrobial chemotherapy of infected wounds. Pharmaceutics 7, 397–412.
887 Chen, H., Li, L., Liu, Y., Wu, M., Xu, S., Zhang, G., Qi, C., Du, Y., Wang, M., Li, J., Huang, X.,
888 2018. In vitro activity and post-antibiotic effects of linezolid in combination with
889 fosfomycin against clinical isolates of Staphylococcus aureus. Infect. Drug Resist. 11,
890 2107–2115.
891 Chiou, S.H., Wu, W.T., 2004. Immobilization of Candida rugosa lipase on chitosan with
892 activation of the hydroxyl groups. Biomaterials 25, 197–204.
893 Choi, M., Hasan, N., Cao, J., Lee, J., Hlaing, S.P., Yoo, J., 2019. Chitosan-based nitric oxide-
894 releasing dressing for anti-biofilm and in vivo. Int. J. Biol. Macromol.
895 Clinmicrorevs, M., Bowler, P., Armstrong, D.G., 2001. Wound microbiology and associated
896 approaches to wound. Clin. Microbiol. Rev. 14, 244–269.
897 Cohen-Sela, E., Chorny, M., Koroukhov, N., Danenberg, H.D., Golomb, G., 2009. A new double
898 emulsion solvent diffusion technique for encapsulating hydrophilic molecules in PLGA
899 nanoparticles. J. Control. Release 133, 90–95.
900 de Carvalho, F.G., Magalhães, T.C., Teixeira, N.M., Gondim, B.L.C., Carlo, H.L., dos Santos,
901 R.L., de Oliveira, A.R., Denadai, Â.M.L., 2019. Synthesis and characterization of
902 TPP/chitosan nanoparticles: Colloidal mechanism of reaction and antifungal effect on C.
903 albicans biofilm formation. Mater. Sci. Eng. C 104.
904 Doern, G. V., Jones, R.N., Pfaller, M.A., Kugler, K.C., Beach, M.L., 1999. Bacterial pathogens

isolated from patients with skin and soft tissue infections: Frequency of occurrence and antimicrobial susceptibility patterns from the SENTRY Antimicrobial Surveillance Program (United States and Canada, 1997). Diagn. Microbiol. Infect. Dis. 34, 65–72.

Donnelly, R.F., Garland, M.J., Morrow, D.I.J., Migalska, K., Raghu, T., Singh, R., Majithiya, R., Woolfson, A.D., 2010. Optical coherence tomography is a valuable tool in the study of the effects of microneedle geometry on skin penetration characteristics and in-skin dissolution. J. Control. Release 147, 333–341.

Donnelly, R.F., Moffat, K., Alkilani, A.Z., Vicente-Pérez, E.M., Barry, J., McCrudden, M.T.C., Woolfson, A.D., 2014. Hydrogel-forming microneedle arrays can be effectively inserted in skin by self-application : A pilot study centred on pharmacist intervention and a patient information leaflet. Pharm. Res. 31, 1989–1999.

Duckworth, P.F., Rowlands, R.S., Barbour, M.E., Maddocks, S.E., 2018. A novel flow-system to establish experimental biofilms for modelling chronic wound infection and testing the efficacy of wound dressings. Microbiol. Res. 215, 141–147.

El-Mohri, H., Wu, Y., Mohanty, S., Ghosh, G., 2017. Impact of matrix stiffness on fibroblast function. Mater. Sci. Eng. C 74, 146–151.

Eskitoros-Togay, M., Bulbul, Y.E., Tort, S., Demirtaş Korkmaz, F., Acartürk, F., Dilsiz, N., 2019. Fabrication of doxycycline-loaded electrospun PCL/PEO membranes for a potential drug delivery system. Int. J. Pharm. 565, 83–94.

Flemming, H.C., Wingender, J., 2010. The biofilm matrix. Nat. Rev. Microbiol. 8, 623–633.

Folsom, J.P., Baker, B., Stewart, P.S., 2011. In vitro efficacy of bismuth thiols against biofilms formed by bacteria isolated from human chronic wounds. J. Appl. Microbiol. 111, 989–996.

González-Vázquez, P., Larrañeta, E., McCrudden, M.T.C., Jarrahian, C., Rein-Weston, A.,

928 Quintanar-Solares, M., Zehrung, D., McCarthy, H., Courtenay, A.J., Donnelly, R.F., 2017.
929 Transdermal delivery of gentamicin using dissolving microneedle arrays for potential
930 treatment of neonatal sepsis. J. Control. Release 265, 30–40.
931 Guo, J., Wang, W., Hu, J., Xie, D., Gerhard, E., Nisic, M., Shan, D., Qian, G., Zheng, S., Yang,
932 J., 2016. Synthesis and characterization of anti-bacterial and anti-fungal citrate-based
933 mussel-inspired bioadhesives. Biomaterials 85, 204–217.
934 Haidar, N.B., Marais, S., Dé, E., Schaumann, A., Barreau, M., Feuilloley, M.G.J., Duncan, A.C.,
935 2020. Chronic wound healing : A specific antibiofilm protein-asymmetric release system.
936 Mater. Sci. Eng. C 106.
937 Hammond, A.A., Miller, K.G., Kruczek, C.J., Dertien, J., Colmer-Hamood, J.A., Griswold, J.A.,
938 Horswill, A.R., Hamood, A.N., 2011. An in vitro biofilm model to examine the effect of
939 antibiotic ointments on biofilms produced by burn wound bacterial isolates. Burns 37, 312–
940 321.
941 Han, C., Romero, N., Fischer, S., Dookran, J., Berger, A., Doiron, A.L., 2017. Recent
942 developments in the use of nanoparticles for treatment of biofilms. Nanotechnol. Rev. 6,
943 383–404.
944 Hasan, N., Cao, J., Lee, J., Hlaing, S.P., Oshi, M.A., Naeem, M., Ki, M.H., Lee, B.L., Jung, Y.,
945 Yoo, J.W., 2019. Bacteria-targeted clindamycin loaded polymeric nanoparticles: Effect of
946 surface charge on nanoparticle adhesion to MRSA, antibacterial activity, and wound
947 healing. Pharmaceutics 11.
948 Høiby, N., Bjarnsholt, T., Givskov, M., Molin, S., Ciofu, O., 2010. Antibiotic resistance of
949 bacterial biofilms. Int. J. Antimicrob. Agents 35, 322–332.
950 Larrañeta, E., Moore, J., Vicente-Pérez, E.M., González-Vázquez, P., Lutton, R., Woolfson,

A.D., Donnelly, R.F., 2014. A proposed model membrane and test method for microneedle insertion studies. Int. J. Pharm. 472, 65–73.

Levy, S.B., Bonnie, M., 2004. Antibacterial resistance worldwide: Causes, challenges and responses. Nat. Med. 10, S122− S129.

Lipsky, B.A., Hoey, C., 2009. Topical antimicrobial therapy for treating chronic wounds. Clin. Infect. Dis. 49, 1541–1549.

Lutton, R.E.M., Larrañeta, E., Kearney, M.C., Boyd, P., Woolfson, A.D., Donnelly, R.F., 2015. A novel scalable manufacturing process for the production of hydrogel-forming microneedle arrays. Int. J. Pharm. 494, 417–429.

Lynch, A.S., Robertson, G.T., 2008. Bacterial and fungal biofilm infections. Annu. Rev. Med. 59, 415−428.

Machul, A., Mikołajczyk, D., Regiel-Futyra, A., Heczko, P.B., Strus, M., Arruebo, M., Stochel, G., Kyzioł, A., 2015. Study on inhibitory activity of chitosan-based materials against biofilm producing Pseudomonas aeruginosa strains. J. Biomater. Appl. 30, 269–278.

Marion-Ferey, K., Pasmore, M., Stoodley, P., Wilson, S., Husson, G.P., Costerton, J.W., 2003. Biofilm removal from silicone tubing: An assessment of the efficacy of dialysis machine decontamination procedures using an in vitro model. J. Hosp. Infect. 53, 64–71.

McCrudden, M.T.C., Alkilani, A.Z., McCrudden, C.M., McAlister, E., McCarthy, H.O., Woolfson, A.D., Donnelly, R.F., 2014. Design and physicochemical characterisation of novel dissolving polymeric microneedle arrays for transdermal delivery of high dose, low molecular weight drugs. J. Control. Release 180, 71–80.

McCrudden, M.T.C., Larrañeta, E., Clark, A., Jarrahian, C., Rein-Weston, A., Lachau-Durand, S., Niemeijer, N., Williams, P., Haeck, C., McCarthy, H.O., Zehrung, D., Donnelly, R.F.,

2018. Design, formulation and evaluation of novel dissolving microarray patches containing a long-acting rilpivirine nanosuspension. J. Control. Release 292, 119–129.

Mihai, M.M., Preda, M., Lungu, I., Gestal, M.C., Popa, M.I., Holban, A.M., 2018. Nanocoatings for chronic wound repair—modulation of microbial colonization and biofilm formation. Int. J. Mol. Sci. 19.

Mili, B., Das, K., Kumar, A., Saxena, A.C., Singh, P., Ghosh, S., Bag, S., 2018. Preparation of NGF encapsulated chitosan nanoparticles and its evaluation on neuronal differentiation potentiality of canine mesenchymal stem cells. J. Mater. Sci. Mater. Med. 29, 1–13.

Mohan, M., Nigam, V.K., Poddar, R., 2019. Towards characterization of bacterial colonies and biofilms: An approach based on swept source optical coherence tomography. Optik (Stuttg). 185, 592–598.

Moore, K., McCallion, R., Searle, R.J., Stacey, M.C., Harding, K.G., 2006. Prediction and monitoring the therapeutic response of chronic dermal wounds. Int. Wound J. 3, 89–96.

Mundargi, R.C., Srirangarajan, S., Agnihotri, S.A., Patil, S.A., Ravindra, S., Setty, S.B., Aminabhavi, T.M., 2007. Development and evaluation of novel biodegradable microspheres based on poly(d,l-lactide-co-glycolide) and poly(ε-caprolactone) for controlled delivery of doxycycline in the treatment of human periodontal pocket: In vitro and in vivo studies. J. Control. Release 119, 59–68.

Noel, S.P., Courtney, H.S., Bumgardner, J.D., Haggard, W.O., 2010. Chitosan sponges to locally deliver amikacin and vancomycin: A pilot in vitro evaluation. Clin. Orthop. Relat. Res. 468, 2074–2080.

Öcal, H., Arica-Yegin, B., Vural, I., Goracinova, K., Çaliş, S., 2014. 5-Fluorouracil-loaded PLA/PLGA PEG-PPG-PEG polymeric nanoparticles: Formulation, in vitro characterization

997 and cell culture studies. Drug Dev. Ind. Pharm. 40, 560–567.
998 Olsen, I., 2015. Biofilm-specific antibiotic tolerance and resistance. Eur. J. Clin. Microbiol.
999 Infect. Dis. 34, 877–886.
1000 Özcan, I., Azizoğlu, E., Şenyiğit, T., Özyazici, M., Özer, Ö., 2013. Comparison of PLGA and
1001 lecithin/chitosan nanoparticles for dermal targeting of betamethasone valerate. J. Drug
1002 Target. 21, 542–550.
1003 Parsons, R., Summers, S., 2017. The role of case studies in effective data sharing, reuse and
1004 impact. IASSIST Q. 40, 14. https://doi.org/10.29173/iq397
1005 Patel J.B., Cockerill R.F., Bradford A.P., Eliopoulos M.G., Hindler A.J., Jenkins G.S., Lewis
1006 S.J., Limbago B., Miller A.L., Nicolau P.D., Pwell M., Swenson M.J., Traczewski M.M.,
1007 Turnidge J.D., W.P.M.Z.L.B., 2015. Methods for Dilution Antimicrobial Susceptibility
1008 Tests for Bacteria That Grow Aerobically; Approved Standard—Tenth Edition. CLSI
1009 (Clinical Lab. Stand. Institute) 35.
1010 Permana, A.D., McCrudden, M.T.C., Donnelly, R.F., 2019a. Enhanced intradermal delivery of
1011 nanosuspensions of antifilariasis drugs using dissolving microneedles: A proof of concept
1012 study. Pharmaceutics 11, 346.
1013 Permana, A.D., Tekko, I.A., McCarthy, H.O., Donnelly, R.F., 2019b. New HPLC–MS method
1014 for rapid and simultaneous quantification of doxycycline, diethylcarbamazine and
1015 albendazole metabolites in rat plasma and organs after concomitant oral administration. J.
1016 Pharm. Biomed. Anal. 170, 243–253.
1017 Permana, A.D., Tekko, I.A., McCrudden, M.T.C., Anjani, Q.K., Ramadon, D., McCarthy, H.O.,
1018 Donnelly, R.F., 2019c. Solid lipid nanoparticle-based dissolving microneedles: A promising
1019 intradermal lymph targeting drug delivery system with potential for enhanced treatment of

lymphatic filariasis. J. Control. Release 316, 34–52.

Rabea, E.I., Badawy, M.E.T., Stevens, C. V., Smagghe, G., Steurbaut, W., 2003. Chitosan as antimicrobial agent: Applications and mode of action. Biomacromolecules 4, 1457–1465.

Roche, E.D., Woodmansey, E.J., Yang, Q., Gibson, D.J., Zhang, H., Schultz, G.S., 2019. Cadexomer iodine effectively reduces bacterial biofilm in porcine wounds ex vivo and in vivo. Int. Wound J. 16, 674–683.

Sader, H.S., Jones, R.N., Silva, J.B., 2002. Skin and soft tissue infections in Latin American medical centers: Four-year assessment of the pathogen frequency and antimicrobial susceptibility patterns. Diagn. Microbiol. Infect. Dis. 44, 281–288.

Said, S.S., Aloufy, A.K., El-Halfawy, O.M., Boraei, N.A., El-Khordagui, L.K., 2011. Antimicrobial PLGA ultrafine fibers: Interaction with wound bacteria. Eur. J. Pharm. Biopharm. 79, 108–118.

Said, S.S., El-Halfawy, O.M., El-Gowelli, H.M., Aloufy, A.K., Boraei, N.A., El-Khordagui, L.K., 2012. Bioburden-responsive antimicrobial PLGA ultrafine fibers for wound healing. Eur. J. Pharm. Biopharm. 80, 85–94.

Smith, A.W., 2005. Biofilms and antibiotic therapy: Is there a role for combating bacterial resistance by the use of novel drug delivery systems? Adv. Drug Deliv. Rev. 57, 1539–1550.

Szomolay, B., Klapper, I., Dockery, J., Stewart, P.S., 2005. Adaptive responses to antimicrobial agents in biofilms. Environ. Microbiol. 7, 1186–1191.

Tato, M., López, Y., Morosini, M.I., Moreno-Bofarull, A., Garcia-Alonso, F., Gargallo-Viola, D., Vila, J., Cantón, R., 2014. Characterization of variables that may influence ozenoxacin in susceptibility testing, including MIC and MBC values. Diagn. Microbiol. Infect. Dis. 78,

263–267.

Vora, L.K., Vavia, P.R., Larrañeta, E., Bell, S.E.J., Donnelly, R.F., 2018. Novel nanosuspension-based dissolving microneedle arrays for transdermal delivery of a hydrophobic drug. J. Interdiscip. Nanomedicine 3, 89–101.

Wolcott, R.D., Rumbaugh, K.P., James, G., Schultz, G., Phillips, P., Yang, Q., Waiters, C., Stewart, P.S., Dowd, S.E., 2010. Biofilm maturity studies indicate sharp debridement opens a timedependent therapeutic window. J. Wound Care 19, 320−328.

Xiong, M.H., Bao, Y., Yang, X.Z., Wang, Y.C., Sun, B., Wang, J., 2012. Lipase-sensitive polymeric triple-layered nanogel for “on-demand” drug delivery. J. Am. Chem. Soc. 134, 4355–4362.

Zhang, Y., Huo, M., Zhou, J., Xie, S., 2010a. PKSolver: An add-in program for pharmacokinetic and pharmacodynamic data analysis in Microsoft Excel. Comput. Methods Programs Biomed. 99, 306–314.

Zhang, Y., Huo, M., Zhou, J., Zou, A., Li, W., Yao, C., Xie, S., 2010b. DDSolver: An add-in program for modeling and comparison of drug dissolution profiles. AAPS J. 12, 263–271.

BUKTI ACCEPTED

Universitas Hasanuddin

Andi Dian Permana <andi.dian.permana@farmasi.unhas.ac.id>

Fwd: Your Submission

1 message

Andi Permana <apermana01@qub.ac.uk> Tue, Apr 4, 2023 at 3:49 PM
To: Andi Dian Permana <andi.dian.permana@farmasi.unhas.ac.id>

Get Outlook for iOS

From: Ryan Donnelly <R.Donnelly@qub.ac.uk>
Sent: Monday, March 9, 2020 2:07:44 AM
To: Andi Permana <apermana01@qub.ac.uk>
Subject: Fw: Your Submission

Congratulations Dian,

Another one for your ever-growing collection.

Very well done!

Ryan

Professor Ryan F. Donnelly
Chair in Pharmaceutical Technology
School of Pharmacy
Queen's University Belfast
Medical Biology Centre
97 Lisburn Road
Belfast
BT9 7BL
UK
Tel: +44 (0) 2890 972 251
Fax: +44 (0) 2890 247 794
Email: r.donnelly@qub.ac.uk

From: eesserver@eesmail.elsevier.com <eesserver@eesmail.elsevier.com> on behalf of International Journal of Pharmaceutics <eesserver@eesmail.elsevier.com>
Sent: 08 March 2020 16:23
To: Ryan Donnelly
Subject: Your Submission

This message is from an external sender. Please take care when responding, clicking links or opening attachments.

Ms. Ref. No.: IJP-D-19-02770R1
Title: Bacterially sensitive nanoparticle-based dissolving microneedles of doxycycline for enhanced treatment of bacterial biofilm skin infection: A proof of concept study
International Journal of Pharmaceutics or its open access mirror

Dear Professor Donnelly,

I am pleased to confirm that your paper Bacterially sensitive nanoparticle-based dissolving microneedles of

doxycycline for enhanced treatment of bacterial biofilm skin infection: A proof of concept study has been accepted for publication in International Journal of Pharmaceutics or its open access mirror

Upon transfer of your paper to our production department, your article proof will be created and sent to you for checking. You will also be asked to complete a number of online forms required for publication. If we need additional information from you during the production process, we will contact you.

Thank you for submitting your work to this journal.

With kind regards,

Juergen Siepmann, PhD
Editor-in-Chief
International Journal of Pharmaceutics or its open access mirror